BRNO UNIVERSITY OF TECHNOLOGY

VYSOKÉ UČENÍ TECHNICKÉ V BRNĚ

FACULTY OF MECHANICAL ENGINEERING

FAKULTA STROJNÍHO INŽENÝRSTVÍ

INSTITUTE OF PHYSICAL ENGINEERING

ÚSTAV FYZIKÁLNÍHO INŽENÝRSTVÍ

DETECTION OF DNA/RNA FRAGMENTS USING GRAPHENE SENSOR AND INFLUENCE OF UPPER ELECTROLYTIC GATE

DETEKCE FRAGMENTŮ DNA/RNA POMOCÍ GRAFENOVÉHO SENZORU A VLIV HORNÍHO ELEKTROLYTICKÉHO HRADLA

BACHELOR'S THESIS

BAKALÁŘSKÁ PRÁCE

AUTHOR — **Kristína Herzánová**

AUTOR PRÁCE

SUPERVISOR — **doc. Ing. Miroslav Bartošík, Ph.D.**

VEDOUCÍ PRÁCE

BRNO 2022

BRNO UNIVERSITY OF TECHNOLOGY
FACULTY OF MECHANICAL ENGINEERING

Assignment Bachelor's Thesis

Institut:	Institute of Physical Engineering
Student:	**Kristína Herzánová**
Degree programm:	Physical Engineering and Nanotechnology
Branch:	no specialisation
Supervisor:	**doc. Ing. Miroslav Bartošík, Ph.D.**
Academic year:	2021/22

As provided for by the Act No. 111/98 Coll. on higher education institutions and the BUT Study and Examination Regulations, the director of the Institute hereby assigns the following topic of Bachelor's Thesis:

Detection of DNA/RNA fragments using graphene sensor and influence of upper electrolytic gate

Brief Description:

Graphene has properties suitable for utilization in biosensors, e. g. high mobility of charge carriers, ultra–sensitivity of electronic properties on individual adsorbed atoms (molecules), the possibility of changing the type of charge carriers by gate voltage in a field effect transistor (FET) arrangement and as a carbon allotrope it is also compatible with biological compounds [1,2]. The aim of this work is to test the electronic response of graphene to organic substances based on deoxyribonucleic / ribonucleic acid (DNA / RNA) [3]. In doing so, the response to different concentrations of these substances and different ways of transport response measurement in the FET arrangement with the lower solid–state and upper electrolytic gates will be mapped [4, 5].

Bachelor's Thesis goals:

1. Literature search of the mentioned problem with emphasis on the possibility of detection of the mentioned compounds by means of non–functionalized graphene.

2. Measure the electronic response to different concentrations of DNA / RNA fragments, namely cytosine.

3. Measure the resistance response in different electronic connections of the FET–basedgraphene biosensor, e.g.
a. without gate,
b. with an upper electrolytic gate,
c. with a lower solid–state gate.
d. study the influence of upper electrolytic gate distance
e. suggest a method for mapping the potential of electrolytic double layer using upper gate.

4. Analyze and discuss the results obtained by individual methods of measurement and compare with similar results in the literature.

Recommended bibliography:

CASTRO NETO, A. H., F. GUINEA, N. M. R. PERES, K. S. NOVOSELOV a A. K. GEIM. The electronic properties of graphene. Reviews of Modern Physics. 2009, 81(1), 109-162. ISSN 0034-6861. Dostupné z: doi:10.1103/RevModPhys.81.109

SCHEDIN, F., A. K. GEIM, S. V. MOROZOV, E. W. HILL, P. BLAKE, M. I. KATSNELSON a K. S. NOVOSELOV. Detection of individual gas molecules adsorbed on graphene. Nature Materials. 2007, 6(9), 652-655. ISSN 1476-1122. Dostupné z: doi:10.1038/nmat1967

HWANG, Michael Taeyoung, Mohammad HEIRANIAN, Yerim KIM, et al. Ultrasensitive detection of nucleic acids using deformed graphene channel field effect biosensors. Nature Communications. 2020, 11(1), 1543. ISSN 2041-1723. Dostupné z: doi:10.1038/s41467-020-15330-9.

BARTOŠÍK, Miroslav, Jindřich MACH, Jakub PIASTEK, David NEZVAL, Martin KONEČNÝ, Vojtěch ŠVARC, Klaus ENSSLIN a Tomáš ŠIKOLA. Mechanism and Suppression of Physisorbed-Water-Caused Hysteresis in Graphene FET Sensors. ACS Sensors. 2020, 5(9), 2940-2949. ISSN 2379-3694. Dostupné z: doi:10.1021/acssensors.0c01441

TRIPSKÝ, Andrej. Design, fabrication and testing of graphene biosensors. Brno, 2020. Diplomová práce. Vysoké učení technické v Brně, Fakulta strojního inženýrství, Ústav fyzikálního inženýrství.

Deadline for submission Bachelor's Thesis is given by the Schedule of the Academic year2021/22

In Brno,

L. S.

prof. RNDr. Tomáš Šikola, CSc. Director of the Institute	doc. Ing. Jaroslav Katolický, Ph.D. FME dean

Abstract

Graphene's unique properties, such as biocompatibility, high charge carrier mobility and surface sensitivity, make it a suitable material for biosensing devices. This thesis aims to describe and demonstrate such sensors and the measurements performed to detect fragments of DNA, specifically cytosine-based substances. The graphene is employed in field-effect transistors as the conductive sensing channel. The doping of graphene induced by adsorbed molecules on the channel causes changes in graphene's transport properties. These changes are reflected in electronic response measurements: real-time measurements of graphene sheet resistance responding to the addition of different solutions and dependency of the resistance to the continual change of gate voltage. The latter can be performed either in the back-gated or electrolytic top-gated configuration of the FET sensor. The difference between the two configurations was observed, as well as the effect of the distance between graphene and top-gate electrode on the sensor response. The results of these measurements are transfer curves exhibiting typical peaks indicating the charge neutrality point (Dirac point) of graphene. Different concentrations of the analyte solution results in different shift of the Dirac point voltage, quantifying the doping level.

Abstrakt

Jedinečné vlastnosti grafenu, jako je biokompatibilita, vysoká mobilita nosičů náboje a povrchová citlivost, z něj činí vhodný materiál pro biosenzory. Cílem této práce je popsat a představit takové senzory a měření provedená za účelem detekce fragmentů DNA, konkrétně látek na bázi cytosinu. Grafen je v polem řízených tranzistorech zapojen jako vodivý snímající kanál. Dopování grafenu vyvolané adsorpcí molekul na vodivém kanálu způsobuje změny transportních vlastností grafenu. Tyto změny se odrážejí v měření elektronických odezev: měření odporu grafenové vrstvy reagujícího v reálném čase na přidávání různých roztoků a závislost odporu na průběžné změně napětí hradla. Druhou metodu měření lze provádět buď v konfiguraci FET senzoru se spodním nebo elektrolytickým horním hradlem. Byl sledován rozdíl mezi oběma konfiguracemi a také vliv vzdálenosti mezi grafenem a horní hradlovou elektrodou na odezvu senzoru. Výsledkem těchto měření jsou transferové křivky vykazující typické píky označující bod neutrality (Diracův bod) grafenu. Různé koncentrace roztoku analytu vedou k různým posunům napětí v Diracově bodě, což kvantifikuje úroveň dopování.

Keywords

graphene, biosensor, field-effect transistor, charge transport, Dirac point, doping, nucleic acids, cytosine

Klíčová slova

grafen, biosenzor, polem řízený tranzistor, transport náboje, Diracův bod, dopování, nukleové kyseliny, cytosin

HERZÁNOVÁ, K. *Detekce fragmentů DNA/RNA pomocí grafenového senzoru a vliv horního elektrolytického hradla.* Brno: Vysoké učení technické v Brně, Fakulta strojního inženýrství, 2022. 42 s. Vedoucí doc. Ing. Miroslav Bartošík, Ph.D.

I declare that I have written the Bachelor's Thesis titled "Detection of DNA/RNA fragments using graphene sensor and influence of upper electrolytic gate" independently, under the guidance of the advisor and using exclusively the technical references and other sources of information cited in the thesis and listed in the comprehensive bibliography at the end of the thesis.

As the author I furthermore declare that, with respect to the creation of this Bachelor's Thesis, I have not infringed and copyright or violated anyone's personal and/or ownership rights. In this context, I am fully aware of the consequences of breaking Regulation § 11 of the Copyright Act No. 121/2000 Coll. of the Czech Republic, as amended, and of any breach of rights related to intellectual property or introduced within amendments to relevant Acts such as the Intellectual Property Act or the Criminal Code, Act No. 40/2009 Coll., Section 2, Head VI, Part 4.

Kristína Herzánová

First, I would like to thank my supervisor, doc. Ing. Miroslav Bartošík, Ph.D., for his guidance, the assistance he provided me during the interpretation of results, and his never-dying patience. I would like to acknowledge Ing. Vojtěch Švarc, Ing. Jakub Piastek and Bc. Linda Supalová for their time, advice, assistance and technical support in the fabrication of the sensors and with the experimental setup. On this note, my thanks also go to anyone else from the Institute of Physical Engineering who helped me along the road in any way. My highest gratitude goes to my family, friends and classmates for their care and moral support that got me through all of the hardships.

Kristína Herzánová

Contents

Introduction **3**

1 Theory **5**
1.1 Graphene and its properties . . . 5
1.2 Graphene synthesis . . . 8
1.2.1 Chemical vapour deposition . . . 8
1.2.2 Other methods . . . 9
1.3 Doping of graphene . . . 10
1.3.1 Electric field-effect doping . . . 10
1.3.2 Surface transfer doping . . . 10
1.3.3 Electrochemical doping . . . 11
1.4 Nucleic acid fragments . . . 12
1.4.1 Structure of nucleic acids . . . 12
1.4.2 Interaction of nucleobases with graphene . . . 13
1.5 Graphene field-effect transistor . . . 14
1.5.1 Back-gated GFETs . . . 15
1.5.2 Top-gated GFETs . . . 16
1.5.3 GFET characteristics and the detection mechanism . . . 17
1.6 Literature review . . . 19

2 Experiment and results **23**
2.1 Sensor design and fabrication . . . 23
2.2 Experimental setup . . . 24
2.3 Characterization by Raman spectroscopy . . . 25
2.4 Biochemical analytes . . . 27
2.5 Transfer curve measurements . . . 28
2.6 Real-time response measurements . . . 30
2.7 Influence of top gate distance . . . 32

Conclusion **35**

Bibliography **37**

List of symbols, quantities and abbreviations **41**

Introduction

Graphene is a two-dimensional carbon semiconductor without a band gap. Although this material was already theoretically described in 1947 by Philip Russell Wallace [1] as one of the atomically thin layers that, when stacked, create graphite. It was only after a few decades when graphene was first isolated from graphite in 2004 by a mere scotch tape by Novoselov et al. [2]. Until then free-standing graphene layer had not been thought to be thermodynamically stable enough to exist. However, despite being only one atom thick and unprotected from the environment, graphene remains stable under ambient conditions. Therefore, the discovery was a breakthrough moment for research in the field of two-dimensional crystals, opening up new possibilities and promising wide applications in electronics. Today, graphene is at the forefront of cutting-edge science and technology due to its exceptional properties.

Because of its structure, graphene is remarkably flexible and at the same time strong, adsorbs only a small fraction of visible light, has high thermal conductivity and high mobility of charge carriers. All of these properties can be exploited, e.g. for the production of transistors, energy storage devices, sensors, transparent conductive layers, or photovoltaic cells.

On top of all that, graphene can be advantageously used in diagnostic medicine as part of biosensors thanks to its biocompatibility, ability to be easily functionalized, ambipolar character and extremely high sensitivity to adsorbed molecules caused by its high surface to volume ratio. Specifically, field-effect transistor-based detection of biomolecules is desirable and has drawn great attention as a label-free molecular sensing platform since the transistors can be readily integrated with other electronic components, such as data analyzers and signal transducers.

The field-effect transistors utilizing graphene as its sensing channel are able to function as electronic sensors working on a principle of resistance changes caused by adsorbed molecules acting as acceptors or donors. In this work, sensors in field-effect transistor arrangement based on physisorption without the possibility of selectively distinguishing only one specific substance are presented and used for the detection of cytosine-based DNA fragments.

1. Theory

1.1 Graphene and its properties

Graphene is a two-dimensional material formed by a single layer of carbon atoms arranged in a hexagonal honeycomb-like lattice. Its structure is depicted in Fig. 1.1a.

The graphene primitive unit cell consists of two atoms, A and B. The bond length between these atoms is 1.42 Å. The Bravais lattice of graphene is a superposition of two triangular sublattices described by primitive vectors $\vec{a}_1$, $\vec{a}_2$. The carbon atoms of one sublattice are connected to three atoms from the other sublattice via equal length bonds $\vec{\delta}_i$ ($i = 1, 2, 3$), which are rotated by 120 °.

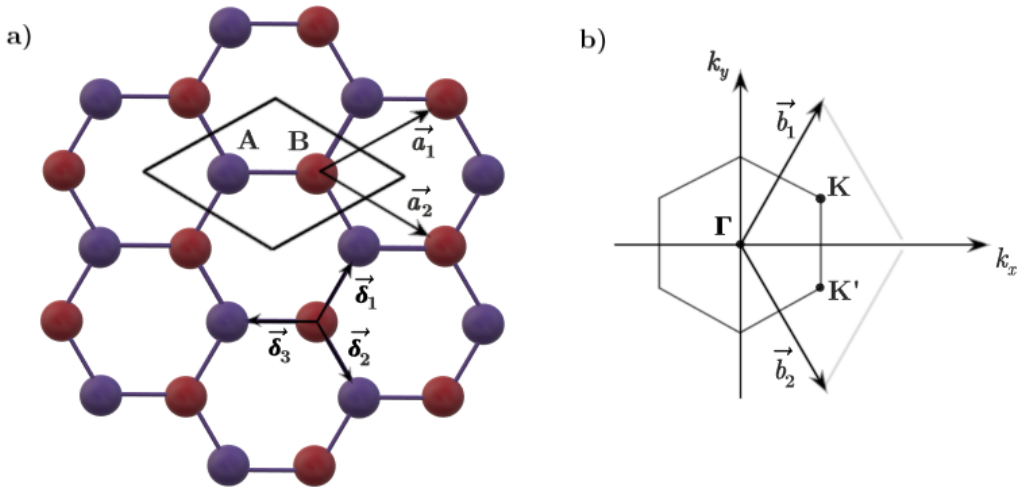

Figure 1.1: a) Hexagonal lattice of graphene. b) The first Brillouin zone of the reciprocal lattice defined by vectors $\vec{b}_1$ and $\vec{b}_2$.

The ground state electron configuration of carbon is given by $1s^2\,2s^2\,2p^2$ (Fig. 1.2a), making it an atom with four valence electrons. In the first excited state, one electron is promoted from the 2s orbital to the 2p orbital. The carbon atoms in graphene are sp^2-hybridized (Fig. 1.2b). This means that valence-shell 2s orbital is combined with two valence-shell 2p orbitals, $2p_x$ and $2p_y$, to form three equivalent hybrid orbitals. These directional hybrid orbitals provide their electrons for the formation of strong covalent

σ bonds between neighbouring carbon atoms, as shown in Fig 1.2c. The remaining valence electron not involved in the binding of atoms occupies the unhybridized $2p_z$ orbital perpendicular to the graphene plane.

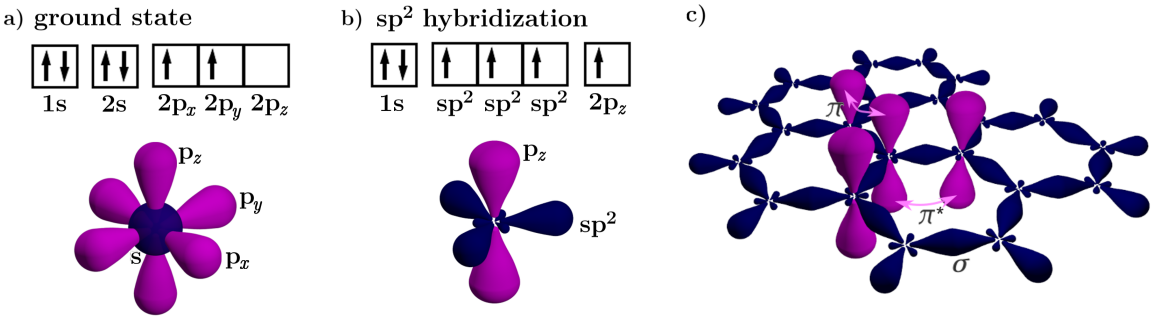

Figure 1.2: The electron configuration of a carbon atom in a) ground state and b) sp^2-hybridized state. c) σ bonds in graphene as overlaps of the hybridized orbitals; p_z orbitals creating π bonds. [3, 4]

The strong σ bonds formed by the carbon atoms are responsible for excellent mechanical properties of pristine graphene [5]. It is the strongest material ever measured, 100 times stronger than steel [6], with intrinsic tensile strength of $\sigma_{\text{int}} = 130\,\text{GPa}$ and extremely large Young modulus of $E = 1.0\,\text{TPa}$ [7]. At the same time, graphene can be easily stretched and bent. However, the presence of defects like dislocations and grain boundaries can significantly influence its plastic deformation and fracture.

Overlap of the protruding unhybridized p_z orbitals results in delocalization of the electrons from these orbitals along the plane of the graphene surface to form long-range conjugated systems. This way, a valence (π) and conduction (π*) bands originate. Since the $2p_z$ orbital of each atom has only one electron, the valence band is completely filled, and the conduction band is empty. That is, graphene has half-filled bands. The electrons in these bands are responsible for the optical and electronic properties of graphene.

The energy spectrum of graphene as a function of the momentum vector $\vec{k} = (k_x, k_y)$ is shown in Fig. 1.3. The momentum vector $\vec{k}$ belongs to the first Brillouin zone of graphene reciprocal lattice shown in Fig. 1.1b. The points at the edge of the first Brillouin zone K and K' near the energy $E = 0$ are high symmetry points referred to as Dirac points. In pristine graphene, the Fermi level (E_F) intersects these points. The spectrum near these points is given by linear dispersion

$$E = \pm v_\text{F} \hbar q, \tag{1.1}$$

where the wavevector $\vec{q}$ is measured from the Brillouin zone vertex K, $q = |\vec{k} - \vec{K}|$, and $v_\text{F} \approx 1.1 \times 10^8\,\text{cm}\cdot\text{s}^{-1}$ is Fermi velocity of graphene [8]. The positive energy branch indicates the conduction band, and the negative energy branch indicates the valence

band. The conduction and valence band touch in Dirac points, therefore, graphene is considered a zero bandgap semiconductor. This determines most of the optical, electronic, and transport properties of graphene.

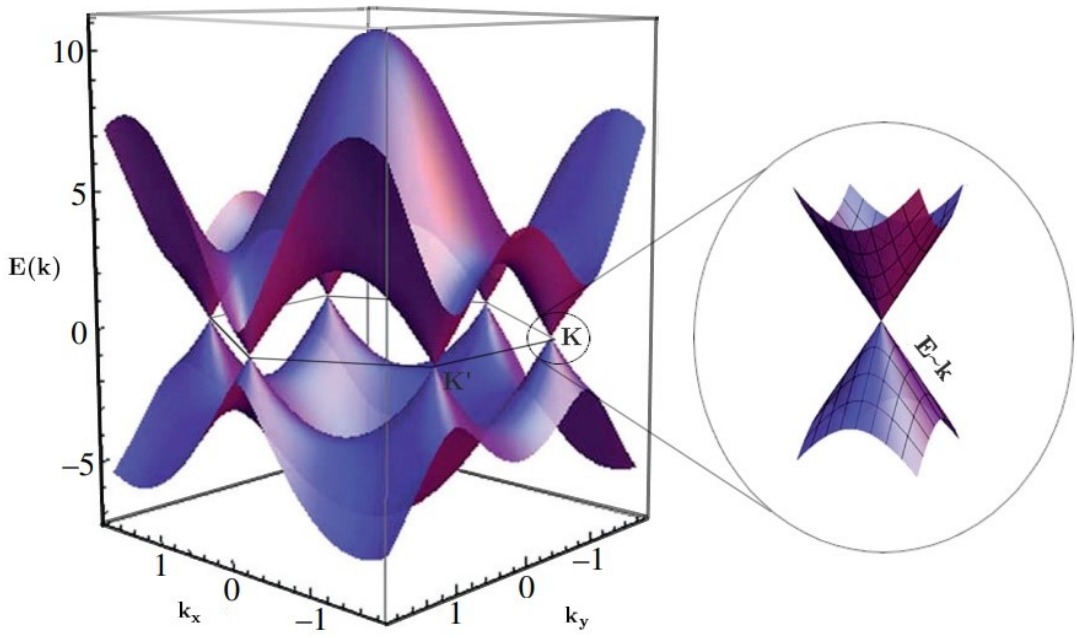

Figure 1.3: The electronic band structure of graphene (left) and detail of the linear part close to Dirac point (right). Adapted from [9].

While in conventional semiconductors, the spectrum is parabolic, in graphene, it is linear (equation 1.1), which accounts for some of the one-of-a-kind electronic properties. From this point of view, the charge carriers in graphene act as relativistic massless particles with an effective speed equal to the Fermi velocity v_F. Therefore, their transport is governed by the relativistic Dirac equation instead of the Schrödinger equation commonly used to describe quantum systems, where the quantum relativistic effects are negligible.

If the graphene lattice contains only a small number of scattering centres such as defects or adsorbed molecules, ballistic transport over longer distances occurs, even at room temperature. Consequently, carriers in pure graphene can have long elastic mean free paths up to several μm, resulting in large charge carrier mobilities. In a diffusive transport regime, mobility is a parameter that quantifies transport quality. Intrinsic mobility of suspended graphene can theoretically reach values up to $200\,000\,\mathrm{cm^2V^{-1}s^{-1}}$. On SiO_2 substrates, scattering of electrons by optical phonons of the substrate limits mobility to $40\,000\,\mathrm{cm^2V^{-1}s^{-1}}$ [10].

Graphene conducts very efficiently along its plane, both heat and electricity. Its thermal conductivity exceeds any other material with an exceptional value of 3 500–$5\,000\,\mathrm{Wm^{-1}K^{-1}}$ [11] and so does its electrical conductivity, with a critical current den-

sity of $1 \times 10^8\,\mathrm{Acm}^{-2}$ [12]. Graphene's conductivity never falls below a minimum value corresponding to the quantum conductance unit, even when the charge carrier density is approaching zero [13].

Single-layer graphene adsorbs only approximately 2.3 % of light of all visible wavelengths [14]. The high transparency is caused mainly by its thinnes. However, the optical visibility can be affected by the underlying substrate [15]. A graphene layer on SiO_2 substrate can be seen by the naked eye due to light interference, allowing observations with an ordinary optical microscope.

1.2 Graphene synthesis

1.2.1 Chemical vapour deposition

Chemical vapour deposition (CVD) is the most convenient and relatively inexpensive method for large-scale production of high-quality graphene [16]. It is a technique in which a metal substrate inserted into a reaction chamber is exposed to one or more precursor gases that react or decompose on its surface to form graphene films.

The substrates usually used in CVD are transitional metals. The graphene growth is conducted in two ways, depending on the substrate. The first type of growth is through carbon diffusion and consequent segregation of whole graphene sheets in metals with high carbon solubility (e.g., Ni, Fe). The other type, more preferred in application, is growth initiated by surface adsorption in metals with low carbon solubility (e.g., Cu). In this case, the carbon atoms nucleate and form graphene grains, gradually increasing in size. The process ends when the grains merge and the substrate is fully covered by one graphene layer [17].

As a carbon source serve so-called precursor gases, usually hydrocarbon molecules like methane (CH_4), which is also most popular, or acetylene (C_2H_2). The precursors are introduced into the reaction chamber, leading to decomposition followed by nucleation and graphene growth on a substrate surface.

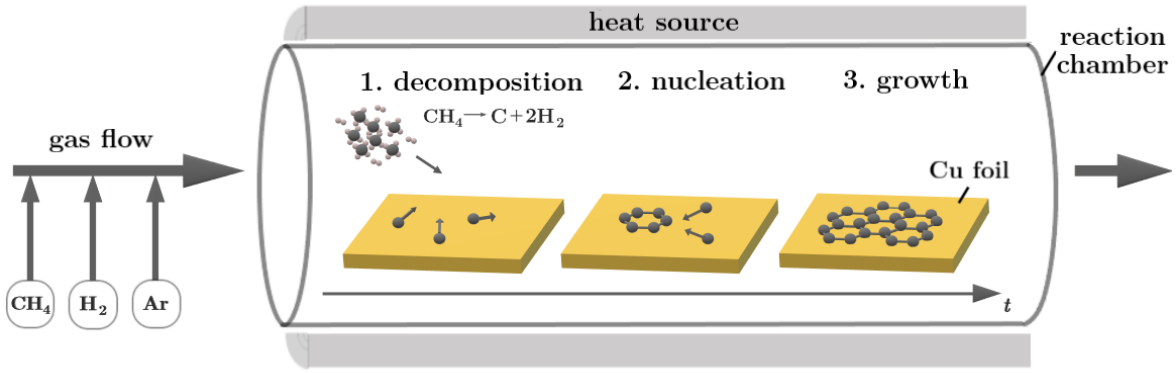

Figure 1.4: Thermal chemical vapour deposition of graphene on copper substrate.

Flown into the reaction chamber along with the precursors are the carrier gases usually composed of hydrogen gas and inert gases such as argon. These gases enhance surface reaction by removing the by-products of ongoing reactions out of the chamber. In order to avoid unwanted results, the flow ratio of methane and hydrogen must be carefully tuned. If not, formation of multilayers can occur.

There are several types of CVD that generally differ in operating conditions, surrounding pressure and temperature, and in the means by which the reactions are initiated. The most common approach is thermal CVD performed under sub-atmospheric pressure. Lowering the pressure improves the thickness uniformity of the deposition, and high temperatures increase the rate of reactions.

In case of thermal CVD, carbon sources decompose into carbon atoms and hydrogen due to the heating of the substrate either directly or by radiation from an external source (heated chamber walls). The temperatures used in research range approximately from 500 °C to 1100 °C [18]. The formation mechanism of graphene growth by the thermal CVD method can be seen in Fig 1.4.

Another type of frequently used CVD method is plasma enhanced CVD (PECVD), where the decomposition of the precursor gases is caused by plasma. The advantage of the PECVD process is that it can be performed under low temperature, low pressure, and low carbon source concentration compared with the thermal CVD process [19].

1.2.2 Other methods

There are several other methods for graphene synthesis, varying in quality, quantity, and costs of the product.

First, graphene can be exfoliated from graphite, a bulk material formed of stacked atomic graphene layers held together by van der Waals interactions. Micromechanical exfoliation, often referred to as the "scotch-tape method", is performed by repeated pealing of highly oriented pyrolytic graphene until single-layer films are created. This is possible, because the interactions between layers are much weaker than the adhesion between scotch tape and the carbon atom plane. The mechanical exfoliation method provides the highest quality graphene flakes up to 10 μm in size [2] with least defects and the best electrical properties, including the highest mobilities [20]. Therefore, graphene obtained by this way is suitable for fundamental studies of graphene properties.

On the other hand, graphene synthesized by liquid-phase exfoliation has low electrical quality. However, the method has the advantage of short, low-cost and large-scale preparation. Liquid-phase exfoliation relies on overcoming the graphite sheet interlayer van der Waals force by using a solvent with suitable intercalating agents, which are molecules that place themselves between layers [21].

Epitaxial growth on SiC is also possible. In this case, graphene nucleates following a controlled sublimation of the Si atoms after thermal decomposition of SiC. After the Si desorption occurs, carbon left on the surface rearranges to form a hexagonal lattice. The process is conducted in ultrahigh vacuum. The main disadvantage of this method is high cost [22].

1.3 Doping of graphene

Charge carriers, either electrons or holes, can be induced in graphene by the application of an electric field or by chemical doping. Chemical doping involves the interactions of graphene with other species. Further, three mechanisms of chemical doping can be distinguished: surface transfer doping, also called adsorption-induced doping, electrochemical doping, and substitutional doping [23].

Electric field-effect doping and electronic surface transfer doping are essential for sensing biomolecules by graphene-based devices. On the other hand, electrochemical doping causes unwanted effects in these devices. These types of doping mechanisms are described in the following sections alongside their consequences.

1.3.1 Electric field-effect doping

The electric field-induced electrostatic doping of graphene is usually performed by later described graphene-based field effect transistors. Pristine graphene exhibits a strong ambipolar electric field effect such that both types of charge carriers, electrons and holes, can be induced by changing the electrical potential between graphene and an isolated electrode on which a voltage is applied. By varying this voltage, the type of carriers and their density in graphene can be tuned. The polarity of the in-graphene induced carriers is opposite to the polarity of the applied voltage. A positive voltage induces electrons while negative voltage induces holes. In other words, the electric field doping transforms graphene into majority electron or hole semiconductor by shifting its Fermi level above or below the Dirac point [24].

1.3.2 Surface transfer doping

By being a two-dimensional material with a high surface to volume ratio, graphene is highly sensitive to surface adsorbates, even to unintentional doping by species adsorbed from the surroundings or residual polymers used during the fabrication [25]. The exposure of different atoms and molecules can modify graphene's electronic properties and result in both n- and p-type doping. Surface doping is non-destructive and does not alter the band structure of graphene, and is mostly reversible, unlike substitutional doping, when some carbon atoms in the lattice are substituted by other atoms with a different number of valence electrons.

In the case of surface transfer doping, the doping is a consequence of direct charge exchange between graphene and dopants adsorbed on the surface. The charge transfer is determined by the relative position of density states (DOS) of the highest occupied molecular orbital (HOMO) and lowest unoccupied molecular orbital (LUMO) of the dopant and the Fermi level of graphene (Fig. 1.5). If the HOMO of a dopant is above the Fermi level of graphene, the dopant acts as a donor and the electrons transfer to graphene. On the other hand, if the LUMO is below the Fermi level, electrons transfer from graphene to the adsorbed molecule takes place, so the dopant acts as an acceptor.

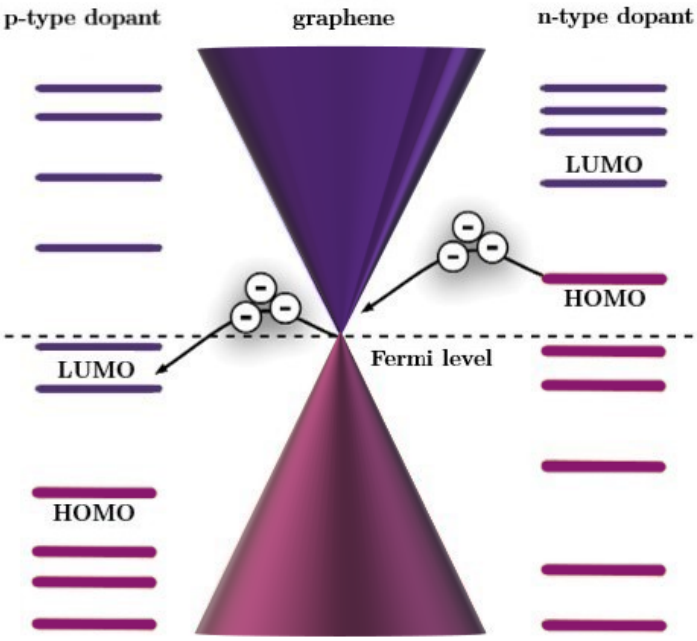

Figure 1.5: The relative position of the highest occupied and lowest unoccupied molecular orbitals of p-type and n-type doping adsorbate to the Fermi level of graphene. Mechanism of surface transfer doping. Adapted from [23].

The Fermi level of graphene, located in the Dirac point in pristine graphene, is shifted due to doping. P-type doping shifts the Fermi level of graphene below the Dirac point, and n-type doping shifts it above. Generally speaking, molecules with electron-withdrawing groups (e.g., water vapour) adsorbed on the graphene surface will lead to p-type doping of graphene, and molecules with donating groups (e.g., ammonia, aromatic molecules) will lead to n-type doping.

1.3.3 Electrochemical doping

The electrochemical doping of graphene occurs when certain surface adsorbates participate in electrochemical redox reactions in which graphene plays the role of an electrode. Whether a reaction will result in p- or n-type doping of graphene depends on the relative position of the electrochemical redox potential E_{redox} to the graphene Fermi level. The E_{redox} is the equivalent of the Fermi level of an electrolyte solution. It measures the energy required to add or remove an electron in redox couples. While the E_{redox} level lies higher (lower) than E_{F}, electrons (holes) induced by a reaction will flow to graphene until equilibrium is reached.

It was observed that the exposure of graphene to a humid atmosphere causes p-type doping, but doping of graphene in the presence of water can't be understood within the surface transfer doping model [23]. In contrast to electronic doping, which occurs instantaneously, electrochemical doping is a time-dependent process which is affected by

the rate of the reaction and diffusion rates of participating species [26]. Electrochemical doping combined with charge trapping and diffusion inside the dielectric substrate is thus the origin of the hysteresis effects often observed in graphene-based electronic devices operating under atmospheric conditions [27].

1.4 Nucleic acid fragments

1.4.1 Structure of nucleic acids

Nucleic acids are the most important macromolecules for all living organisms. They carry the genetic information of a living cell as well as the instructions for its functioning. There are two naturally occurring types of nucleic acids, ribonucleic acid (RNA) and deoxyribonucleic acid (DNA). DNA is the material that encodes genetic information and ensures its preservation, while RNA plays a role mainly in gene expression and is involved in protein synthesis.

Nucleic acids are composed of monomer units called nucleotides forming long polynucleotide chains. The unit length of one molecule can be as much as one billion nucleotides [28]. A nucleotide consists of three components: a nitrogenous base, a five-carbon (pentose) sugar, and a phosphate group (Fig. 1.6).

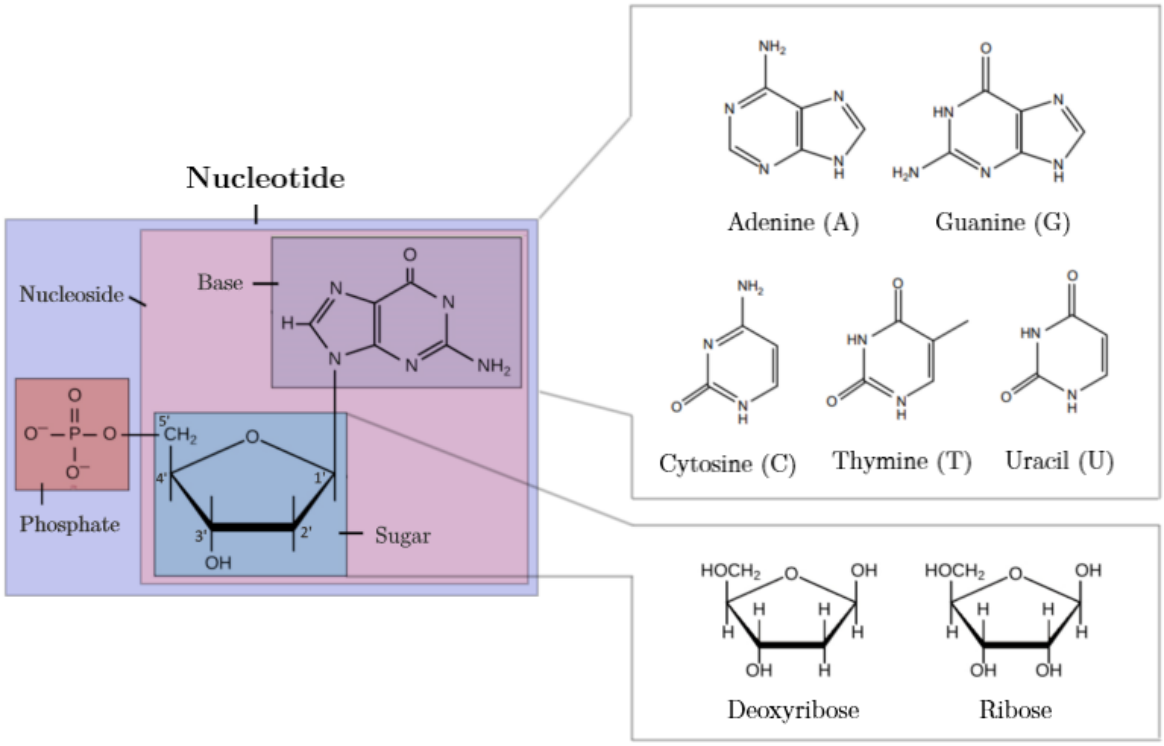

Figure 1.6: Nucleotide, a fundamental structural unit of DNA/RNA, and its components.

The pentose sugar in RNA is D-ribose, while in DNA, it's 2'-deoxy-D-ribose. The difference between the sugars is the presence or absence, respectively, of a hydroxyl (OH) group at the second carbon of the sugar.

A nucleotide in DNA contains one of four possible bases: adenine (A), guanine (G), cytosine (C), and thymine (T). RNA contains the same bases with exception of thymine that is substituted by uracil (U). Bases can be divided into two categories, purines and pyrimidines. Adenine and guanine are classified as purines, molecules made of two carbon-nitrogen rings, and cytosine, thymine and uracil as pyrimidines, which have monocyclic structure. Each of the basic rings has different functional groups attached to it.

Each base in a nucleotide is joined to a sugar by a glycosidic bond to form a nucleoside. The nucleoside derives its name from constituent base and sugar. For example, cytosine and D-ribose form cytidine (C), while cytosine and 2'-deoxy-D-ribose constitute deoxycytidine (dC). The sugar molecule then forms a bond with one or more phosphate groups.

Nucleotides are phosphate esters of nucleosides created by esterification of the hydroxyl group of the sugar by a phosphate residue. The formed molecules are named derivatively from nucleosides. For example cytidine 5'-monophosphate (CMP) is a molecule created out of cytidine esterification of the hydroxyl group of the 5' sugar carbon atom by a single phosphate group (PO_4). In the DNA and RNA strands, the phosphate residue is attached to the hydroxyl group of the 5' carbon of one sugar and of the 3' carbon of the sugar of adjecent nucleoside, forming 5'-3' phosphodiester linkage.

The base order created by the linkages between individual nucleotides is referred to as a primary structure of DNA/RNA and distinguishes one nucleic acid molecule from another. The sequence of the bases encodes genetic information. It is also the primary structure of nucleotide polymers that dictates specific interactions of two nucleic acid molecules in the formation of double-stranded helical structures.

1.4.2 Interaction of nucleobases with graphene

Understanding the DNA-graphene interactions is key to developing graphene-based biosensors for DNA detection. The primary interactions include π-π stacking and electronic interactions (e.g., induced dipoles, doping, chemical gating) [29].

The non-covalent π-π stacking of bases and graphene, shown in (Fig. 1.7a), can be explained within the model of planar interaction of two aromatic rings with conjugated π-bands. Direct stacking of the rings is repulsive as it places two sets of carbon atoms and negatively charged π-electron systems on top of each other. Therefore, the molecules force themselves into an offset geometry until they reach an optimized configuration yielding the minimum total energy when the attractive electrostatic interaction between the negatively charged π-electrons and the positive σ-framework outweighs the π-electron repulsion. Unlike the covalent bonding, the stacking between graphene and bases does not disrupt the conjugated network of graphene and thus, preserves its electronic properties.

Density-functional theory (DFT) calculations [30] shown that in addition to π-π stacking, DNA adsorption induces an interfacial dipole between the nucleobases and graphene (Fig. 1.7b). The dipole is the result of the close association of electron-rich aromatic rings of the bases and the polarizable graphene surface.

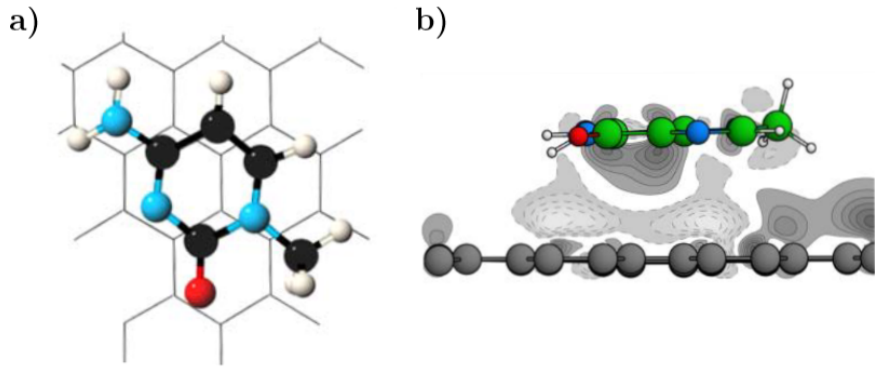

Figure 1.7: a) The equilibrium geometry of cytosine on top of graphene [31]. b) Calculated charge density difference for adsorbed guanine on graphene [30].

1.5 Graphene field-effect transistor

The field-effect transistor (FET) is a device usually used as an amplifier or logical switch. It consists of a conductive channel and three electrodes - source (S), drain (D) and gate (G). A schematic illustration of a general FET is shown in Fig. 1.8. The constant voltage V_{DS} applied between the source and the drain results in an electric current I_{DS}

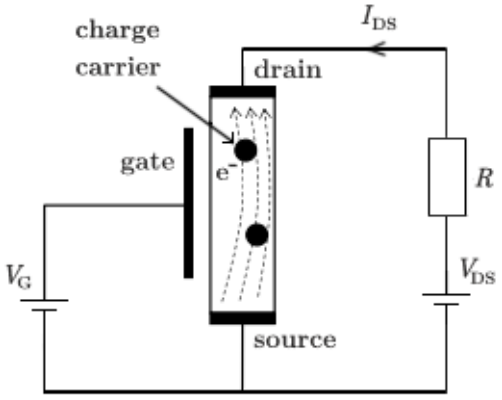

Figure 1.8: Diagram of a general field-effect transistor (with n-type semiconductor channel where the majority charge carriers are electrons). Adapted from [32].

flowing through the channel that is insulated from the gate. The gate is then designated to control the current flow through the channel by a transversal electric field created by applying voltage V_G to the gate. Altering V_G modulates the charge carrier density of the channel. The charge transfer in FETs is always carried out only by one type of carriers, the so-called majority charge carriers, which are holes or electrons.

A graphene field-effect transistor (GFET) implements graphene as the conductive channel. GFET exploits the fact that in graphene, charge carriers can be easily induced by applying gate voltage. Due to graphene's ambipolar character, switching between both types of charge carriers in the channel is possible. Also, having zero bandgap results in high carrier mobility and sensitivity to surface changes of graphene, so GFETs hold promise for use as sensors. GFETs allow the detection of chemical and biological species while also revealing their doping effects on the graphene and the carrier mobility of graphene.

1.5.1 Back-gated GFETs

The back-gated GFET configuration (Fig. 1.9) consists of a graphene layer placed between two electrodes on a solid substrate providing mechanical support to the thin material. The top part of the substrate is made of a dielectric, insulating the source, drain, and graphene channel from the conductive lower part of the substrate that acts as a gate. The most popular substrate for GFETs is degenerately-doped Si covered with a layer of SiO_2 [33].

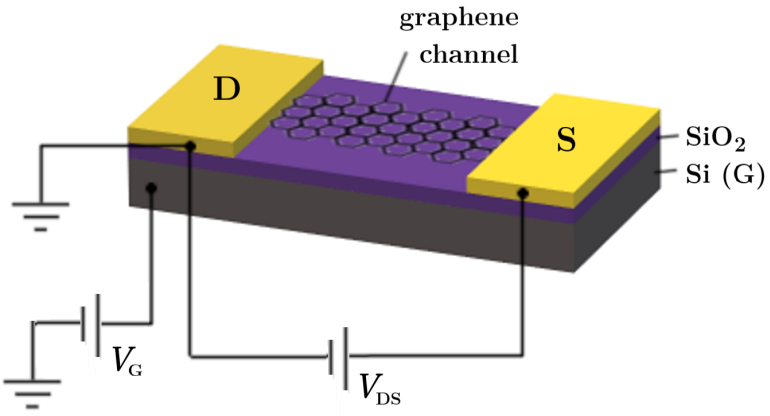

Figure 1.9: Schema of a GFET assembled in a back-gated configuration.

The gate voltage V_G in this setup induces a surface charge density given by equation

$$n = \frac{\epsilon_0 \epsilon_r V_G}{et} \tag{1.2}$$

where ϵ_0 represents vacuum permittivity, ϵ_r the relative permittivity of the dielectric, e the elementary charge and t the thickness of the dielectric layer [2]. This relation

can be obtained by considering the silicon gate and the graphene layer as plates of a parallel-plate capacitor.

Back-gated GFETs require higher gate voltages in the order of tens to hundreds of volts to achieve significant gain. The back-gate is more demanding to fabricate in comparison with the top-gate, therefore, it is employed less frequently for biochemical detection. However, back-gated GFETs have advantage in situations, where the analyte is in the gas phase [29].

1.5.2 Top-gated GFETs

In top-gated GFET (Fig. 1.10a) the sample solution acts as a medium between graphene and the gate. The gate electrode is usually established by a wire inserted into the top of the electrolyte droplet. The gate electrode immersed in an electrolyte containing the target molecules should be made of biocompatible materials, such as Ag/AgCl, Ag, or Pt, in biosensing applications [33].

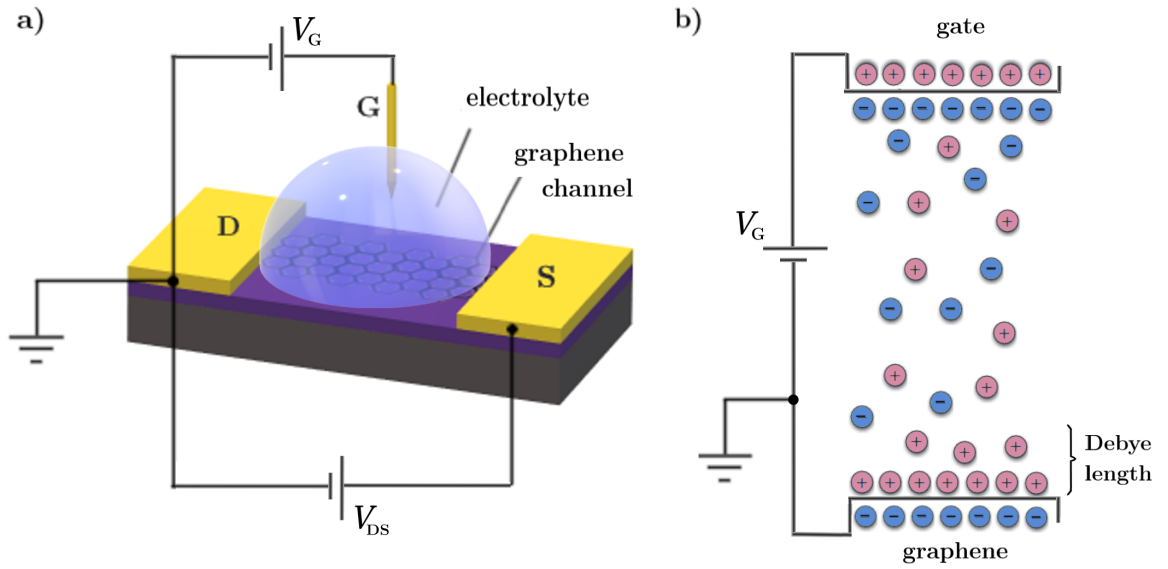

Figure 1.10: a) Schema of a GFET assembled in a top-gated configuration. b) Formation of electrolytic double layer (EDL). Adapted from [34]

An important distinction between back- and top-gated GFETs is the potential for current to flow between the graphene and the gate electrode via the aqueous ionic solution separating the conductive bodies. However, the leakage is limited, at low gate voltages, by the formation of an electrolytic double layer (EDL) along the surface of the graphene and gate electrode due to the voltage bias [34]. Top-gated GFETs are typically operated at voltages in the order of $\pm 1\,\mathrm{V}$. Higher voltages set off electrolytic processes in the solution and lead to high gate currents.

The electrolytic double layer is formed by redistribution of ions in the solution medium due to contact with a charged conducting surface as shown in Fig. 1.10b.

Surface charges cause an electric field that attracts counter ions. The counter ions arrange themselves according to the electric potential near the interface. This potential decreases exponentially with the distance from the charged surface [35]. The decay length is called Debye length and is given by

$$\lambda_{\mathrm{D}} = \sqrt{\frac{\epsilon k_{\mathrm{B}} T}{e^2 N_{\mathrm{A}} \sum \rho_i Z_i}}. \tag{1.3}$$

Here, ϵ is the permittivity of the medium, k_{B} the Boltzmann constant, T the temperature, e the elementary charge, N_{A} the Avogadro's number, and ρ_i and Z_i the density and valence of ion species i respectively [33].

The Debye length determines the spatial range of detection by a GFET. Charged molecules in the solution farther then λ_{D} are screened by the counter ions in the solution and are usually considered out of the detection range. Hence, the larger λ_{D} is, the more molecules from a greater distance can influence the graphene channel, increasing the device sensitivity.

1.5.3 GFET characteristics and the detection mechanism

The detection mechanism of the GFET sensor relies on monitoring alterations of its electrical characteristics caused by the analyte molecules interacting with the graphene channel. Observed differences in measured metrics provide information about the detected molecules.

The drain-source current in the device, commonly recalculated to conductance $G_{\mathrm{DS}} = I_{\mathrm{DS}}/V_{\mathrm{DS}}$ or resistance $R_{\mathrm{DS}} = V_{\mathrm{DS}}/I_{\mathrm{DS}}$, depends on the changes in the density of charge carriers. The density of charge carriers can be modulated by electrostatic doping, caused by the gate voltage V_{G}, and adsorption-induced doping.

FET devices are typically characterized using two standard measurements: current vs. gate bias and current vs. time [33]. The outputs of these measurements are, consequently, transfer curves and time series. The effect of the analyte on such electrical curves can be monitored either by comparing a given metric before and after exposure to the sample, or in real-time by recording dynamic changes.

The transfer curves represent the output drain-source current I_{DS} as a function of the gate voltage V_{G} at a fixed drain-source voltage value V_{DS}. It is obtained by sweeping the gate voltage V_{G} in a given range. A typical V-shaped transfer curve showcasing the ambipolar character of a GFET is shown in Fig. 1.11a. The left branch represents increasing density of positive charge carriers (holes). Whereas the right branch represents negative charge carriers (electrons). The minimum of the channel current, corresponding to minimum conductance and maximum resistance, indicates equal populations of both types of carriers. This is consistent with the Fermi level crossing the Dirac point. The voltage in the transfer curve extreme is referred to as the Dirac point voltage V_{D} or sometimes as charge neutrality point voltage V_{CNP}. Ideally, for undoped pristine graphene, $V_{\mathrm{D}} = 0$.

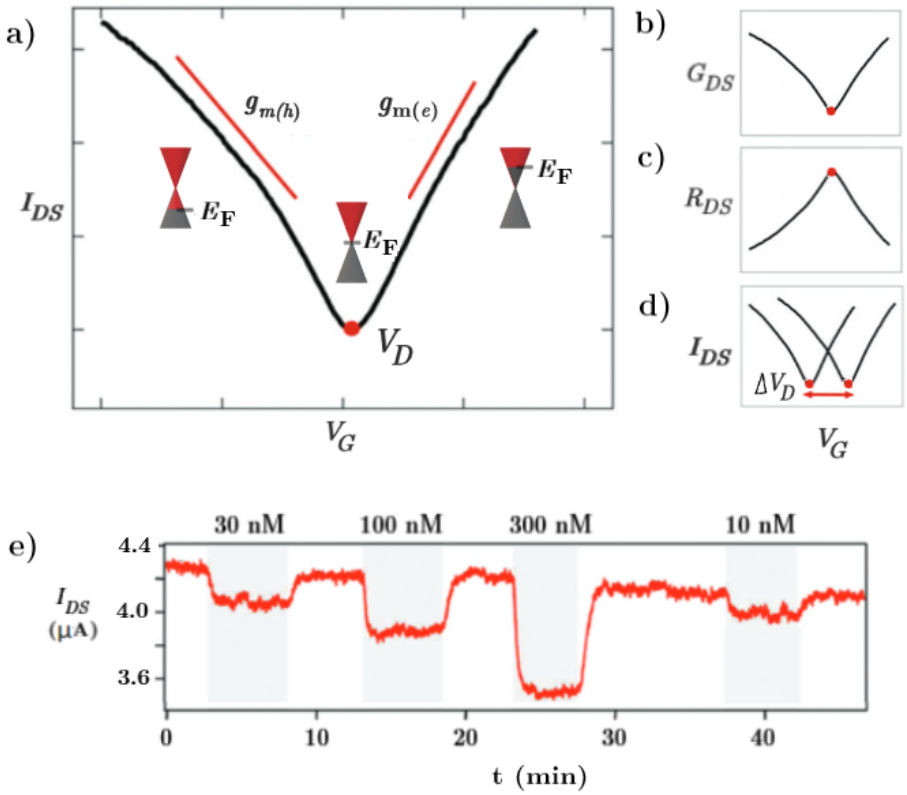

Figure 1.11: Measured characteristics of a GFET sensor. a) Typical transfer curve $I_{DS}(V_G)$ of a GFET, b) $G_{DS}(V_G)$ dependency, c) $R_{DS}(V_G)$ dependency and d) shift of the Dirac point voltage V_D. Adapted from [33]. e) Time series of a GFET sensor for thrombin, recording the introduction of various concentration of analyte separated by washing cycles [36].

The essential information extracted from the measurements of the transfer curves is the shift of the Dirac point voltage ΔV_{D} depending on the induced doping effect of the analyte solution. The shift is indicative of the type and degree of doping. In doped graphene, the Fermi level shifts away from the Dirac point. The Fermi level shift (ΔE_{F}) is defined as the energy difference between the Fermi level and the Dirac point. For p-doped graphene, the Fermi level is below the Dirac point and V_{D} is shifted to the right, and for n-doped graphene, the Fermi level is above the Dirac point and V_{D} is shifted to the left.

The slope of the linear part of the transfer curve g_{m} is called the transconductance and is given by

$$g_{\mathrm{m}} = \frac{W}{L}\mu C_{\mathrm{G}} V_{\mathrm{DS}}, \tag{1.4}$$

where W is the width and L the length of the rectangular graphene channel, μ the charge carrier mobility and C_{G} the gate capacitance. The gate capacitance is determined by the insulating layer separating graphene channel from gate electrode in back-gated configuration and by the EDL, acting similarly as a thin dielectric layer, in top-gated configuration. The transconductance is another characterization speaking

about the transistor performance. For a given device geometry, it is mainly dependent on the mobility μ of charge carriers, which is inversely proportional to the number of impurities in the sample acting as additional scattering sites [33]. Real devices may exhibit different mobility values for electrons and holes, which is partly due to the graphene-electrode contacts [37].

The dynamic real-time measurements for the detection of analytes follow the evolution of the output I_{DS} at a fixed V_{DS} and V_G is monitored as a function of time. Detection of the analyte, and sometimes its quantification, is assessed from the current changes after its introduction. Example of output of such measurement is shown in Fig. 1.11e, where the current flowing through the channel decreases with concentration of target molecules in solution.

1.6 Literature review

Field-effect transistors for bioanalytical sensing first appeared around 1980, adapted from ion-sensitive FETs made for pH sensing. Early FET sensors were made of traditional semiconductors and had limited detection sensitivity. The discovery of low-dimensional semiconductors like graphene, MoS_2, and black phosphorus with high surface to-bulk ratios inspired their use for enhancing the sensitivity of FET sensors. Graphene is by far the most available and well-studied among them, and since its discovery, GFETs were implied as bioanalytical and chemical sensors, for instance, for DNA hybridization, pH or gas molecular (NO_2, NH_3) detection. More recently, research has been mainly focused on developing GFETs for biomolecular detection, including analytes such as glucose, biomarkers, bacteria and viruses, antibiotics, or nucleic acids [33].

Nucleic acid detection is mainly possible due to the graphene-nucleobase interactions. GFETs are often implemented for the detection of DNA hybridization, which is the process of bonding between two single-stranded DNA molecules to form a double-stranded molecule. The bonding depends on the correct base-pairing (A-T and G-C) across the two single-stranded molecules. Alterations in the complementary sequences of bases cause changes in the detected signal. Detection of single-base polymorphism or mutation of DNA is key to the diagnosis of genetic diseases and the realization of personalized medicine.

In 2010 Dong et al. [38] were able to reach the detection of DNA hybridization with single-base specificity. DNA probe molecules for sequence-selective detection were pre-immobilized on CVD graphene placed on a glass substrate by leaving a phosphate-buffered saline (PBS) with dissolved DNA strands for 16 h to allow the saturate attachment to the graphene surface. The ability of the probe DNA immobilization was explained by the domination of the non-electrostatic $\pi-\pi$ stacking. The probe molecules themselves caused a left shift of the Dirac point voltage (V_D) relative to the reference measurement with PBS only, indicating n-doping by the bases. The shift in V_D increased with the increasing concentration of the complementary DNA up to 10 nM,

suggesting that the complementary DNAs can also effectively interact with graphene and impose an n-doping effect based on the graphene-nucleotide interaction. In contrast, the addition of one-base mismatched molecules did not cause a significant shift in V_D.

In the same work, measurements for adenosine (A) and adenosine-5'-triphosphate (ATP) on non-functionalized graphene were carried out. Fig. 1.12 compares the shifts in V_D caused by adsorption of these molecules. Noted that adenosine is a nucleoside with a neutral charge while ATP is adenosine attached with a negatively charged triphosphate group. Despite the charge difference, the two molecules cause a similar left-shift in V_D, indicating that the negative charge in ATP or in DNA is not the cause of a right V_D shift by electrostatic doping effect.

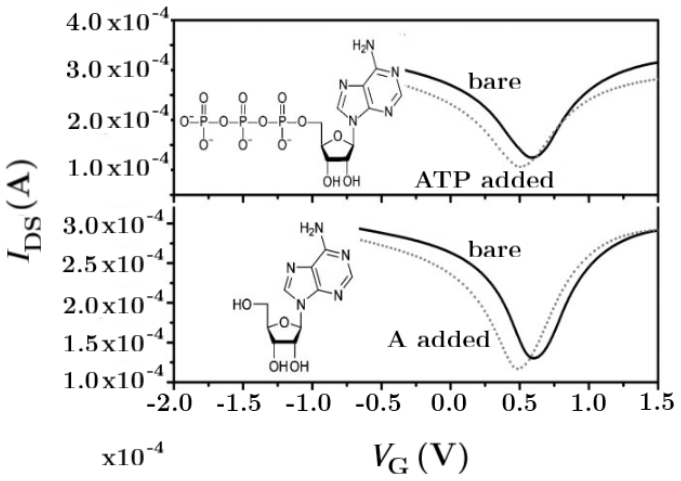

Figure 1.12: Transfer characteristics of the graphene devices before and after adsorption of adenosine-5'-triphosphate (ATP) and adenosine (A) [38]

The following research focused on enhancing the detection limit of hybridization detection by several different methods. Dong et al. [38] and Danielson et al. [39] decorated the GFET graphene channel with gold nanoparticles (AuNPs). AuNPs covalently bind with thiolated DNA molecules acting as receptor molecules. Such functionalized sensor is illustrated in Fig. 1.13a. The formation of AuNPs generally imposes a p-doping effect on the transistors. In [38], the AuNP decoration, performed by immersing graphene films in $HAuCl_4$ solution, enabled an extension of the detection range of DNA hybridization from 10 nM to 500 nM and also allowed detection with one-base mismatch sensitivity. In [39], the biosensors were decorated with AuNPs synthesized from magnetron sputtering inert gas condensing technique to avoid the use of residual reactants that could interfere with the Au-thiol binding present in solvent-based decoration methods. Fig. 1.13b shows the difference between bare and AuNPs decorated sensors. DNA detection at attomolar level was achieved by this novel method.

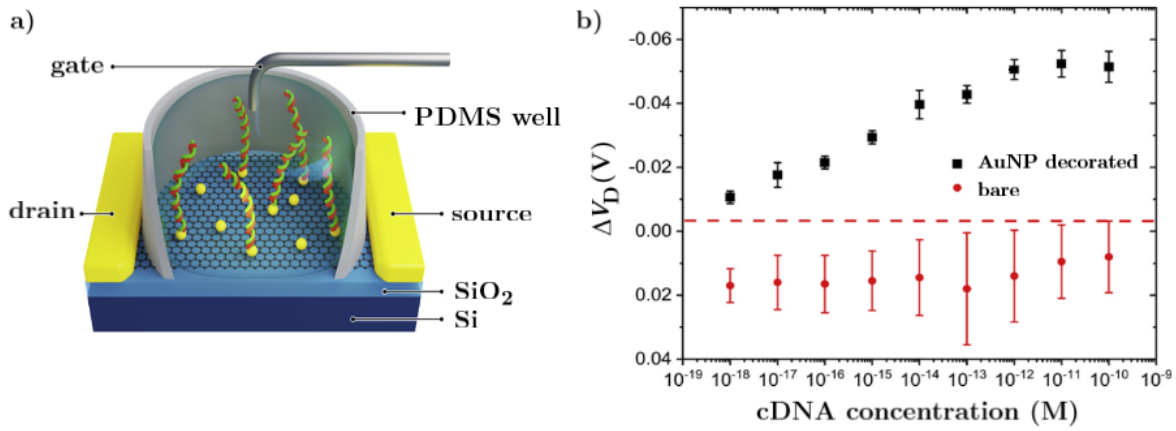

Figure 1.13: a) Schematic diagram of a GFET with AuNPs decoration for DNA sensing in solution. b) The shift of V_D for bare and AuNPs decorated GFET biosensors after exposure to a series of concentrations (from 1 aM to 100 pM) of DNA complementary to the probe molecules [39].

Hwang et al. [40] used GFETs with a deformed monolayer graphene channel for the detection of nucleic acids. The devices showed an ultra-high sensitivity detection in buffer and human serum samples down to 600 zM and 20 aM, respectively, which corresponds ∼18 and ∼600 molecules. The detection limit of FET sensors determined by the screening of the charges from counter ions was enhanced by nanoscale deformations that can form so-called electrical hot spots in the sensing channel, which reduce the screening at the concave regions (Fig. 1.14). The sensing channel was deformed by annealing the graphene on a polystyrene substrate at 110 °C for 4 h. This process induces the shrinkage of the underlying thermoplastic substrate, which results in the buckling of graphene.

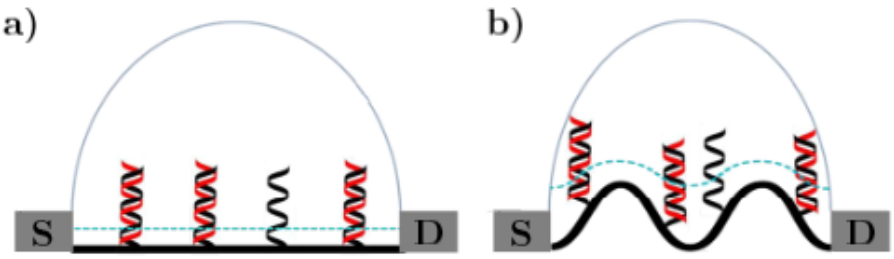

Figure 1.14: Cross-sectional scheme of a) flat and b) deformed GFET sensor. Probe (black) and target (red) DNA strands are immobilized on the surface of graphene. The dotted lines represent Debye length in the ionic solution [40].

Other methods for increasing the detection sensitivity of graphene-based devices include, for example, fabrication of graphene by thermal CVD directly on a sapphire

substrate, avoiding the degradation of electrical properties during graphene transfer, performed by Xu et al. [41]; or room-temperature Ar plasma treatments, proposed by Xia et al. [42], removing residues from the graphene surface and changing its hydrophilic properties.

And While all the aforementioned studies have been carried out using top-gated GFETs, Ping et al. [43] developed biosensors based on a scalable fabrication of arrays of back-gated GFETs. The results of measurements and reached conclusions were similar, only the range over which the V_{D} values shifted due to doping was larger.

2. Experiment and results

The experimental part of this thesis focuses on the utilization of graphene field-effect transistors for the detection of cytosine-based nucleic acid fragments. The results of resistance response measurements of such devices give an insight into how the interactions of graphene with the biochemical samples affect its electronic properties. Two different experimental setups were used to measure the sensor response to various solutions.

2.1 Sensor design and fabrication

A 525 µm thick silicon wafer covered with a 280 nm thick SiO_2 layer was used as the substrate creating the base of the samples used for the electrical transport measurements. The two-probe design of the sensors used in the experiments is shown in Fig. 2.1a. The three pairs of electrodes on the substrate surface were formed by optical lithography, using a focused UV laser beam for direct writing on a positive photoresist AZ 5214 E, followed by development in AR 300-475 and deposition of 5 nm layer of Ti and 80 nm layer of Au by electron-beam evaporation. Resist residues and Ti/Au coating in the areas not exposed to the light were then removed by the "lift-off" process.

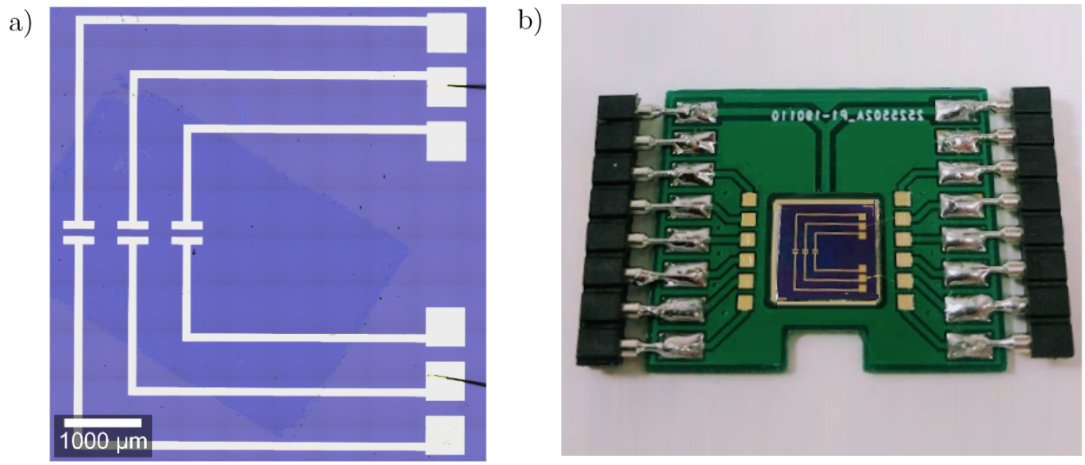

Figure 2.1: Design of the graphene-based sensor. a) Optical microscope image of the sample consisting of Si/SiO_2 substrate patterned with golden electrodes and partially covered by a graphene sheet. b) The sample attached to an expander.

The graphene was synthesized by a standard low-pressure thermal CVD method on Cu foil and coated with a layer of PMMA for structural support. The final sample preparation stage consisted of the graphene transfer onto the patterned substrate to create electrical contact between the golden electrodes by the so-called "wet" transfer method. The process includes multiple steps. First, Cu was etched away by immersing the PMMA/graphene/Cu film in $Fe(NO_3)_3$ solution for 2 hours. Then the released PMMA/graphene film floating on the liquid was washed by moving it in and out of deionized (DI) water by lifting it on a Si/SiO_2 chip. To remove residues on the underside of the graphene sheet, it was left in 5% HCl for 5 minutes. After that, the film was washed in DI water again, transferred onto the sample, and the water remaining under the film was blown out by nitrogen. The layer was then left to dry on the sample for several hours. At last, the dissolution of PMMA on the graphene surface was achieved by immersing the sample in acetone heated to 50 °C for 2 hours, then in IPA to neutralize the acetone and finally in ethanol.

Before the measurement, the sample was annealed at 180 °C for 4 hours, removing some of the water molecules trapped between the graphene and the substrate after long exposure to ambient conditions. This brings the desired effect of higher durability of the graphene sheet by preventing it from excessive tearing during measurements that are often caused by adding or removing drops of aqueous solutions.

The last step of the sensor fabrication is the attachment of the prepared sample with a conductive silver paint onto an expander (Fig. 2.1b), which connects the sample to an electric circuit. The square-shaped ends of the Au electrodes are used as contacting areas for wire-bonding.

2.2 Experimental setup

A diagram of the electric circuit sample setup is shown in Fig. 2.2. To measure the charge transport in graphene, the FET assembly was utilized. Lithographically fabricated structures on the substrate surface form the source and drain electrodes, between which the current flows through a graphene channel. The conductance of the channel can be modified by the gate voltage.

The current passing through the channel was generated by a lock-in amplifier Standford Research SR830 with a 10 MΩ resistor connected in series. Such resistance is much higher compared to the resistance of the sample, preventing it from being damaged. The amplitude of the voltage applied to the graphene layer was set to $V_{DS} = 1\,V$, making the drain-source current $I_{DS} = 100\,nA$. The lock-in amplifier was also used for collecting the signal from the sample to determine the resistance of the graphene sheet.

The gate electrode, either a doped Si substrate or Au wire, was connected to a Keithley 6221 AC/DC current source connected in parallel to a 1 MΩ resistor realizing the gate voltage.

The measurement parameters were controlled via a program designed in the LabView environment, which also serves the purpose of recording and plotting the data

obtained during the measurement.

All of the experiments were carried out under ambient conditions at atmospheric pressure (10^5 Pa) and a room temperature (25 °C).

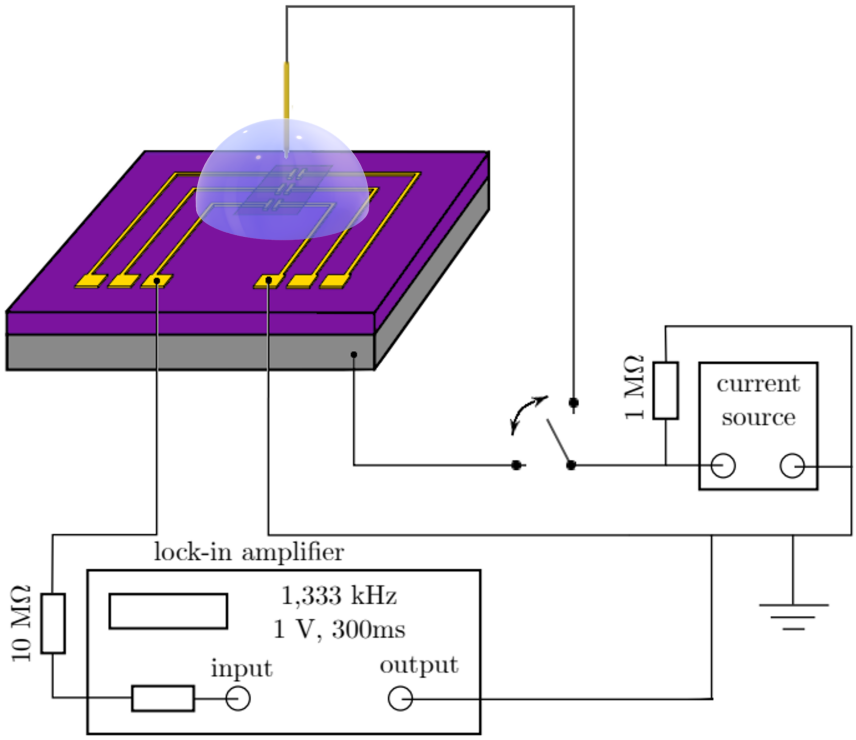

Figure 2.2: Schematic of the electronic setup for transport measurements. Adapted from [27].

2.3 Characterization by Raman spectroscopy

Characterization of graphene by Raman spectroscopy is a non-destructive method often used to indicate graphene's quality. It involves investigating its structure, defects, and determination of the number of graphene layers.

Raman spectroscopy relies upon the inelastic scattering of photons from a monochromatic laser focused on the sample. The photons interact with phonons, atomic vibrations or other excitations in the system, leading to an increase or decrease in their energy. The shift in energy gives information about the vibrational modes in the system. The Raman spectrum usually exhibits three main peaks, namely D, G and 2D. The peak intensities and shapes give a considerable amount of information about the sample. Both D and 2D peaks, located at about 1350 cm^{-1} and 2700 cm^{-1} respectively, originate from second-order Raman scattering that involves two phonons near the Dirac

point. In the case of the D peak, elastic defect-induced scattering and inelastic scattering caused by the emission or absorption of a photon occur. Whereas, for the 2D peak, both processes are inelastic. The G peak appears close to 1580 cm^{-1} and it corresponds to lattice vibrational modes.

To examine the quality of one of the graphene samples used in the experiments performed in this thesis, Raman spectroscopy measurements using a 20 mW laser with excitation wavelength 532 nm were carried out prior to the use of the sensor. Raman spectra taken in 3 different laser spot positions on the sample are shown in Fig. 2.3.

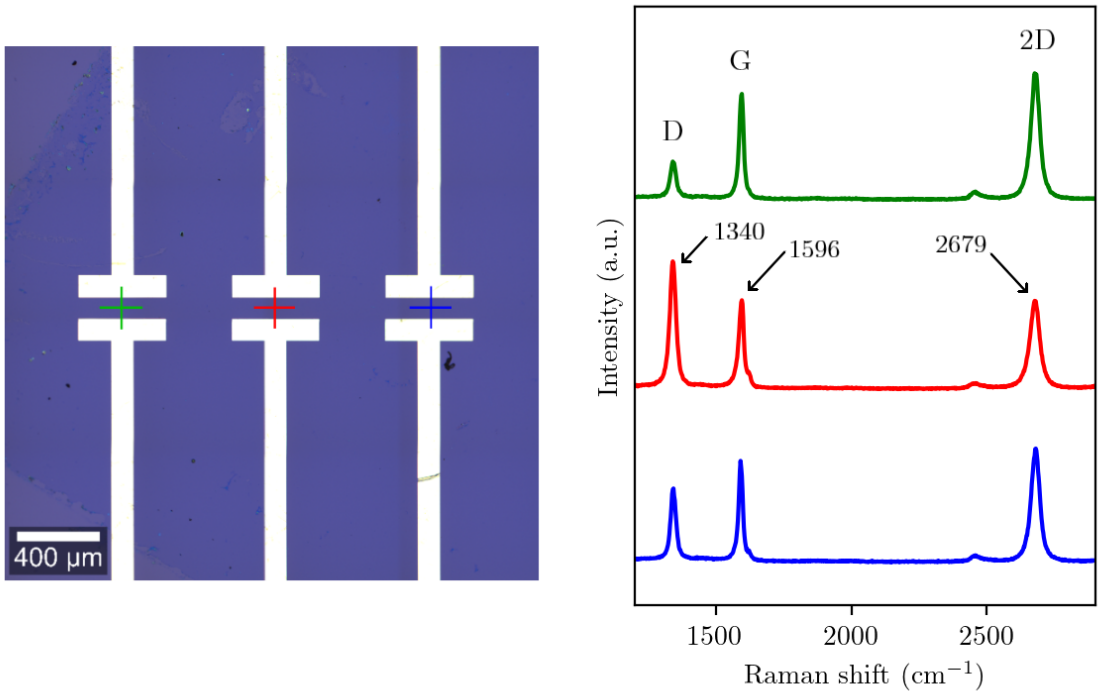

Figure 2.3: Raman spectra (right) of the points in the points marked on the microscope image (left).

In the case of stacking of graphene layers, the 2D Raman bands split. The splitting opens up going from bilayer to multilayer graphene, leading to distortion and broadening of the 2D peak. Judging from the large intensity and sharp shape of the 2D peak (Fig. 2.3), we can state that the sample subjected to the spectroscopy measurement is covered with a monolayer graphene [44].

We can also observe the D peak, typically appearing in a disordered sample or at the graphene edge and sub-domain boundaries, in spectra of each of the positions. The D peak intensity is highest in the spot between the middle pair of electrodes (red cross), implying a higher level of disorder. A small area (20x20 μm^2) around this spot was selected for mapping the distribution of intensity of each peak to give us a better view of the graphene structure (Fig. 2.4).

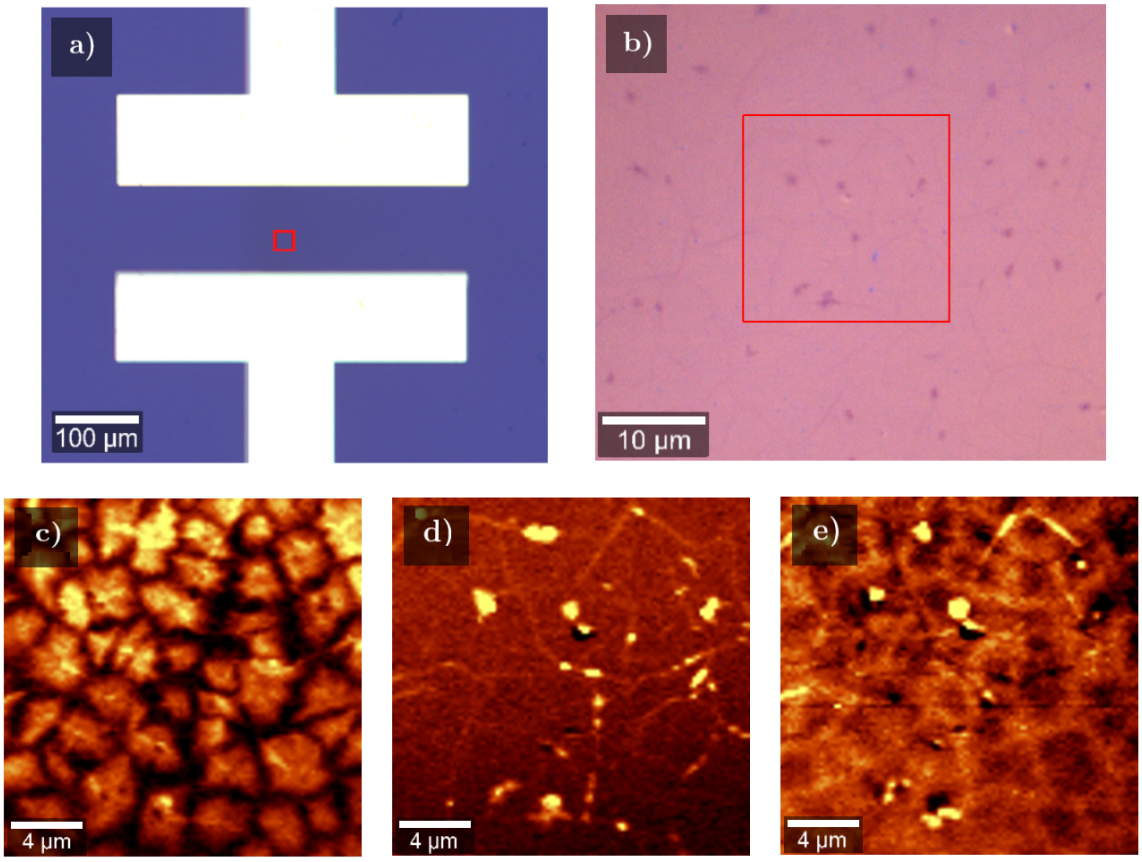

Figure 2.4: a) Selected area of Raman spectroscopy mapping. b) Zoom in on the selected area with adjusted image contrast and brightness. Map of the c) D peak, d) G peak, and e) 2D peak.

2.4 Biochemical analytes

Three different analytes (Fig. 2.5), cytosine (C), deoxycytidine (dC), and cytidine-5'-monophosphate (CMP) were used in the measurements. A set of solutions with concentrations of 0.1 mM, 1 mM, and 10 mM of each substance were provided by the Institute of Biophysics of the Czech Academy of Sciences. The molar concentration represents the amount of the substance dissolved in a unit volume of the solvent, in this case DI water. It is given by the equation

$$c = \frac{n}{V} = \frac{m}{MV} \qquad (\mathrm{mol} \cdot \mathrm{dm}^{-3}, \mathrm{M}), \tag{2.1}$$

where n is the amount of solute in moles, V is the volume of the solution, m is the mass of the solute, and M is the molar mass of the solute.

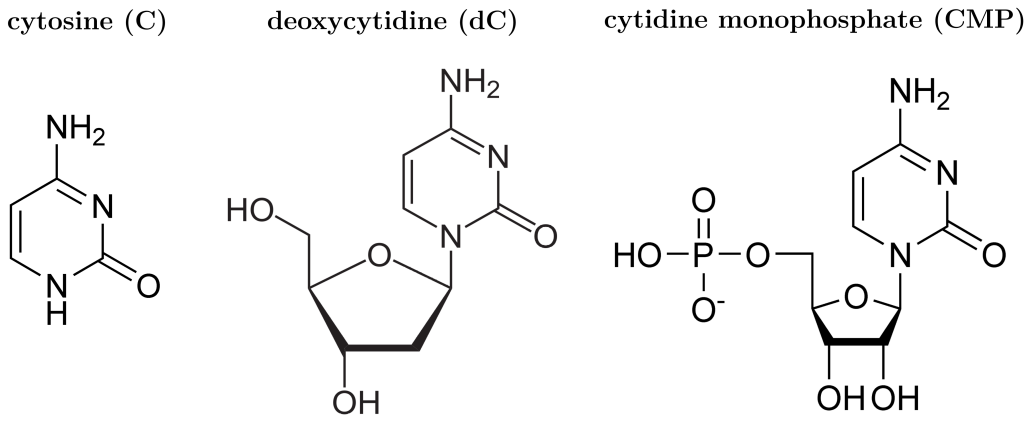

Figure 2.5: Structural formulas of the substances used in the measurements.

2.5 Transfer curve measurements

The main characteristic for the detection of species adsorbed on a sensing channel in the GFETs is the dependency of resistance on the gate voltage. The curves obtained by this type of measurement are called transfer curves and typically exhibit a peak that indicates the crossing of the Fermi level and the Dirac point when the charge carriers are in equilibrium, and the total charge in graphene is therefore zero. The shift of the Dirac point voltage ΔV_{D} corresponding to the maximum resistance value is determined by doping caused by the adsorbed molecules.

The gate voltage applied either by the back gate or the top gate was always continuously swept from 0 V to minimal voltage value, then to maximal voltage value, and finally back to 0 V. A typical curves obtained by such measurements are shown in Fig. 2.6. Here, the top gate realized by a Au wire was immersed into a drop of DI water (blue curve) and a 0.1 mM cytosine solution (red curve). The gate voltage sweep was set in the range of ± 1.5 V with the voltage increment of 0.02 V within one step of duration 0.5 s. The progress of the sweep is marked by the green arrows. The whole transfer curve is shifted due to different doping of the graphene.

As can be seen in the transfer curves, the sensors exhibit a significant hysteresis in atmospheric and water-solution conditions usually observed in real FETs. The hysteresis was observed in both of the sensor configurations. The hysteresis leads to an ambiguity in determination of the peak position such that it is moved to higher voltage values for downward gate voltage sweep, and consequently influences the calculations of the charge carrier concentration and the Dirac point voltage shift. In majority of the measurements, the right peak during the downward voltage sweep was better defined. Therefore, the Dirac point voltage of the right peak was considered when analysing data.

Transfer curves were further measured for C, dC, and CMP with concentrations of 0.1 mM, 1 mM, and 10 mM. The gate voltage in the top-gate was swept as previously described, whereas the voltage in the back-gate configuration was swept with the same

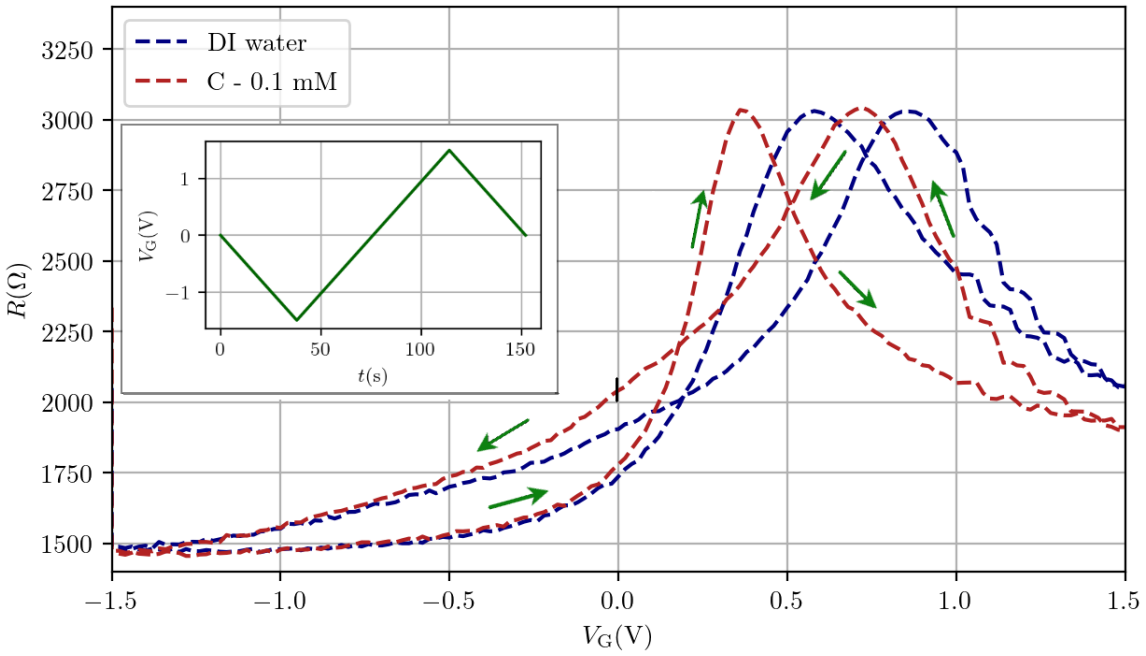

Figure 2.6: The transfer curves for DI water and 1 mM cytosine solution obtained using the top gate with a continual gate voltage sweep (see the inset).

pattern in range of ±50 V and the voltage step was realized with duration of 0.5 s and the voltage increment set to 1 V.

The obtained data were suitably cropped by taking 30 surrounding points around the Dirac point, 15 on the left and 15 on the right, and the data processed in this way were then fitted with polynomials. The data could also be interpolated with a Gaussian curve, but this method proved to be less accurate and in some cases even impossible.

The voltage values corresponding to the extremes of the fitted curves were used for the calculation of the Dirac point voltage shift ΔV_{D}. As a reference value for the calculation of the shift was used the position of Dirac point for DI water. Fig. 2.7 shows the ΔV_{D} for different solutions with concentrations plotted on the logarithmic x-axis of the graph.

The order in which the measurements were performed is in the order of increasing electrolyte concentrations. Between each measurements, the sensor was rinsed with water and IPA and dried with nitrogen.

Based on the results obtained from the transfer curve measurements, we can claim that the graphene sensors were originally majorly p-doped by the DI water, as can be seen in Fig. 2.6, where the resistivity peak is positioned in positive voltage values. A negative shift of the Dirac point was imposed when the cytosine-based solutions were introduced to the channel and caused n-doping respective to the initial doping by DI water.

Most of the measurements suggest that the higher the analyte concentration is, the further the shift is. The only deviation from this tendency applies for the results obtained by the sensor in top-gated configuration for detection of CMP. The polarity

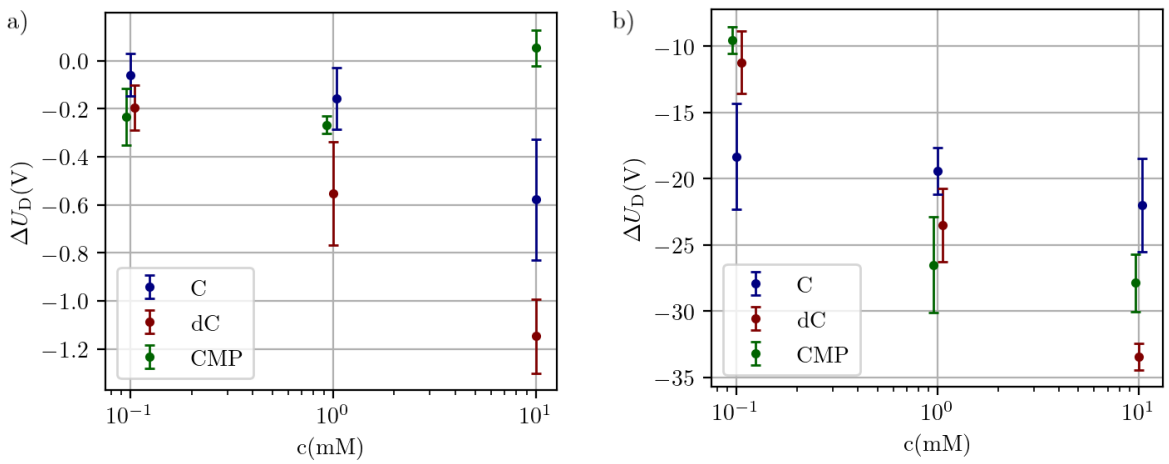

Figure 2.7: Shift of the Dirac point voltage for cytosine-based substances using a) the electrolytic top gate (a) and the b) the solid-state bottom gate (b). Data points were moved fractionally along the x-axis for clarity.

of the shift is however still same. This might be caused by either electrostatic gating by the negatively charged phosphate groups in the nucleotides or the molecules begin interacting with each other, forming electron consuming weak bonds.

Another thing we can also observe from the measurements is that the shift in case of the top-gated sensor is relatively small in comparison to the back-gated one. This is because the gate capacitance of the electic double layer (EDL) formed in the electrolytic top-gated sensor is much larger than that of back-gate dielectrics. That is why gate potentials applied across the EDL can be over two orders of magnitude more efficient than through the back-gate: consequently the sweeping range of gate voltage required is much smaller for gates immersed in the electrolyte compared to the voltage needed for thin oxide insulators in the back-gate [33].

2.6 Real-time response measurements

As the following experimental setup, the real-time sensor response was investigated by measuring the resistance dependency on time without applying gate voltage ($V_G = 0\,V$) while adding different solutions.

Fig. 2.8 shows the time response of the graphene to addition of different concentrations of cytosine solution. The resistance of the graphene channel changed upon the cytosine-graphene interactions.

At $t = 0\,s$, the sensor was in stabilized state in the atmospheric conditions. After 60 s, drop of DI water was added to the channel as a reference. After that, the electrolyte was changed approximately every 5 min. Addition of single droplet caused an immediate steep increase in resistance followed by a slower rise during the stabilization period (Fig. 2.9). Sudden jumps in the graphene resistance correspond to removal and

addition of the 15 µl droplets of the specific solutions. The sensor was rinsed in between by pipetting water on and off several times.

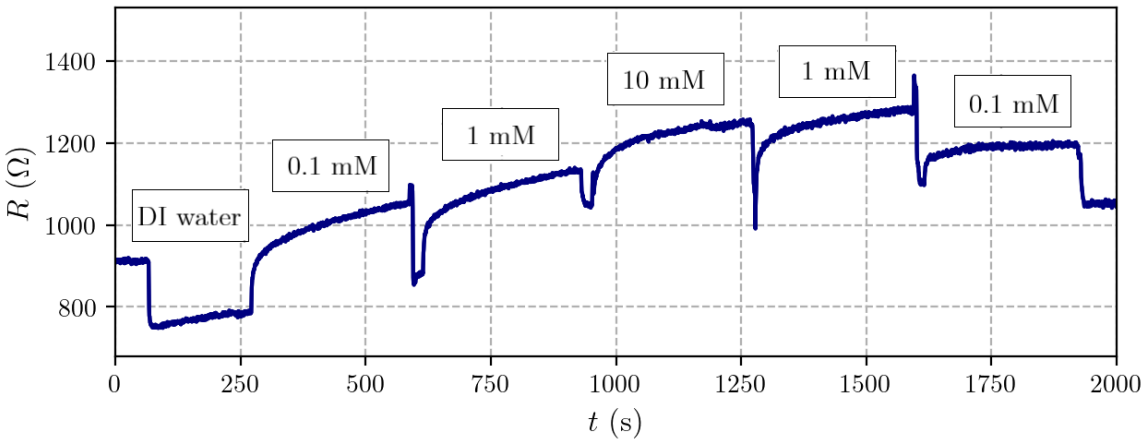

Figure 2.8: Sensor response to different concentrations of cytosine solution.

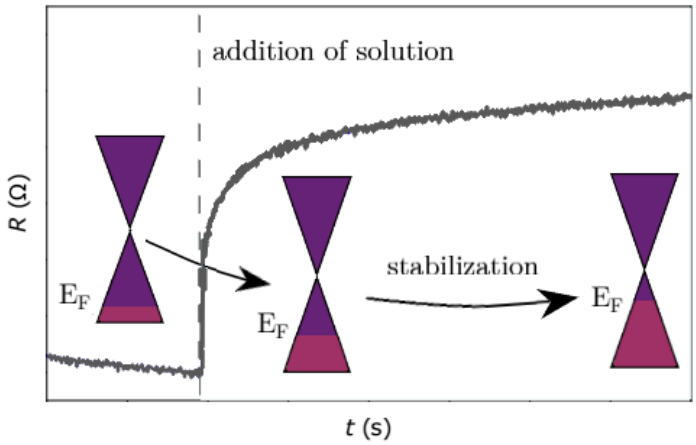

Figure 2.9: The stabilization of the Fermi level after addition of analyte solution. Adapted from [45].

The DI water itself induces p-doping effect in the graphene and the Dirac point voltage V_D value is always positive. For gate voltages higher than V_D for DI water, the Fermi level E_F is shifted below the Dirac point of graphene and for lower voltages, E_F is shifted above the Dirac point. Since the gate voltage was kept at 0 V in the p-doped region of the graphene for the entire measurement, the increase in resistance caused by increase of cytosine concentration indicates n-doping, when the Fermi level is moved back closer to the Dirac point and the number of both types of charge carriers is more balanced. This result agrees with the conclusions acquired from transfer curve measurements.

The same type of measurement as in Fig. 2.8 was also performed for the other two analytes, dC and CMP, and similar behaviour was observed. The sensor always responded with an increase (a decrease) in resistance upon the introduction of solutions with higher (lower) concentrations to the graphene channel. The fact that the resistance of the channel returns to lower values indicates that the interactions between graphene and the analytes are weak and the sensor response is reversible. However, as the concentration decreases, the relative change in resistance is lower, which can be attributed to the accumulation of the molecules due to not being able to always rinse the sensor completely.

If the measurements were to be performed at voltage values higher then V_D for DI water, a drop in resistance with the addition of cytosine would be observed as the Fermi level would shift even further from the Dirac point. Unfortunately, rapid changes of the surface tension due to manipulating with the solution droplets at high voltages would cause tearing of the graphene sheet.

The response of the sensor to different analytes of the same concentration is also presented in Fig. 2.10. More structurally complex molecules cause larger relative resistance changes to the reference level for DI water.

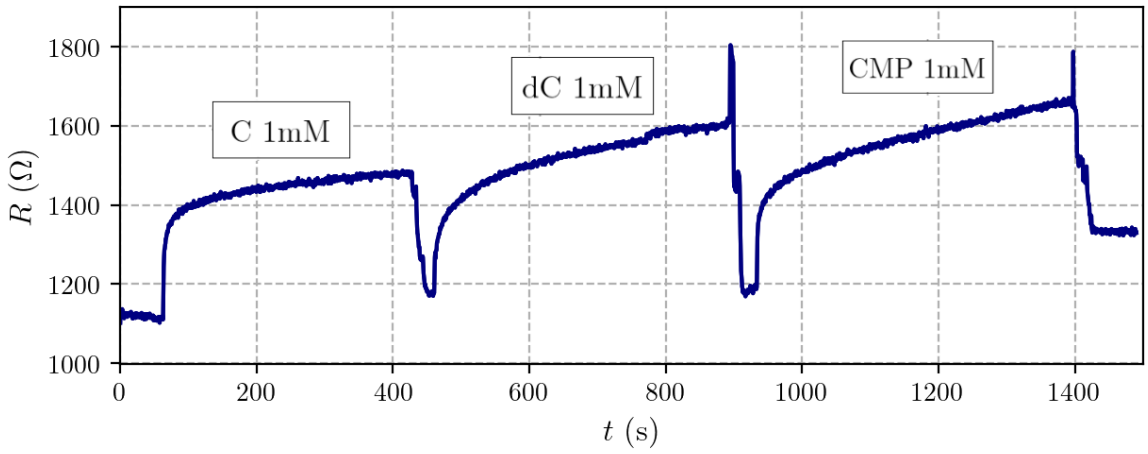

Figure 2.10: Sensor response to different analytes of the same concentration (1 mM).

2.7 Influence of top gate distance

Lastly, in addition to previous commonly performed GFET measurements, the resistance response of the sensor in dependency on the graphene-gate distance in the top-gate configuration was mapped.

The distance between the gate electrode and graphene channel was measured as seen in schema in Fig. 2.11 using a vertically adjustable micrometer feed to which the electrode realized by the wire was firmly fixed. The reference zero distance was measured in position just right next to the graphene sheet so that the tip of the wire

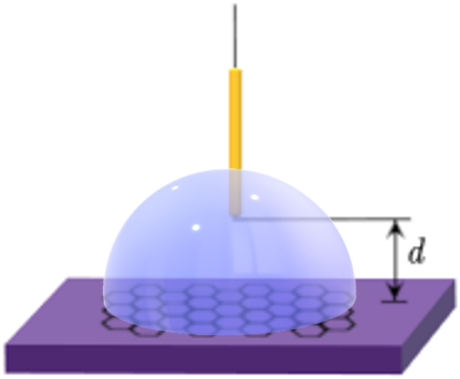

Figure 2.11: Distance between the top-gate electrode and the graphene channel.

would not damage the graphene. The values subsequently read on the micrometre were then subtracted from this reference distance to obtain the distance the wire is from the graphene. Minor uncertainties associated with the experimental assembly might have occurred during the measurement. However, the assembly allows us to at least qualitatively describe what happens.

The results of the real-time measurement are shown in Fig. 2.12a. A 15 µl droplet of 1 mM cytosine solution was added to the sensor. The end of Au wire was first immersed into the droplet from above. The measurement started after addition of the droplet and the gate implementation at $V_G = 0$ V. Then a single 0.5 V top-gate voltage step was applied. This constant value of V_G was maintained until the end of the measurement.

The gate electrode was gradually moved by the micrometer closer to the surface. With every step, the sensor was left for approximately 90 s to stabilize. The dependency of resistance on the graphene-gate distance d was plotted in separate graph shown in Fig. 2.12b. The resistance values were obtained as the maximum resistance in the stabilization period of the sensor.

While approaching the graphene surface with the electrode, the resistance started to change significantly only in the distance approximately below 100 µm. Saturation in the resistance response of the sensor occurs at larger distances.

This suggests that when the gate is closer to the graphene, larger amount of charge carriers are implemented in graphene. This behaviour could be explained within the earlier mentioned capacitor model in chapter 1.5.1.

In the case of immersed gate configuration, the shape and position of the gate electrode can vary considerably, but the capacitance is mostly determined by the electrical double layer (EDL) formed at the graphene surface by reorganization of ions in the electrolyte media and by the screening Debye length [33]. The EDL acts similarly as a very thin dielectric layer in back-gated configuration. The charge carrier density depends on V_G generally as

$$n = \alpha V_G, \tag{2.2}$$

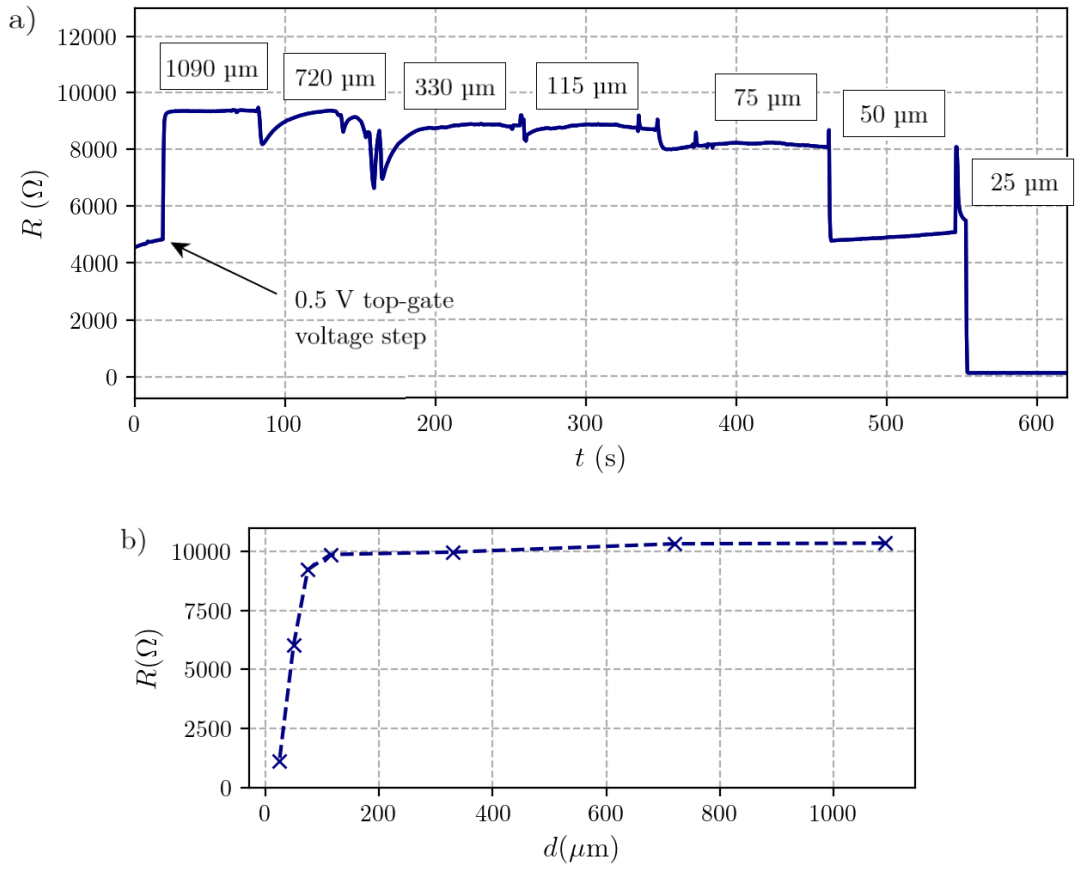

Figure 2.12: a) The real-time resistance response of the sensor to the change of the graphene-gate distance. b) Dependency of the resistance on the distance.

where α is a proportionality constant. For the back gate, the constant is expressed in the equation 1.2. The relation 2.2 also applies for the top-gated configuration. However, the constant α is different and is inversely proportional to the Debye length λ_D given by 1.3. At distances grater then λ_D (outside of the EDL), α is invariant. Since at certain distance the V_G in the experiment is set at a certain value, but n changes, we can assume that the gate electrode disrupts the EDL and imposes an effective λ_D in the electrolyte.

In conclusion, the response of the sensor depends on the gate-graphene distance in the top-gate configuration due to the changes in the ion containing solution behaviour. This finding can serve as a subject to future measurements.

Conclusion

In recent years, research has been focused on the development of graphene field-effect transistors (GFETs) implementing graphene as their conductive channel that serves as a platform for biomolecular detection. The aim of this bachelor's thesis was to theoretically describe and exploit sensors in the GFET configuration for the detection of nucleic acid fragments.

A working biosensor based on the non-functionalized CVD graphene was presented and successfully tested specifically for the detection of three analytes: cytosine (nucleobase), deoxycytidine (nucleoside) and cytidine monophosphate (nucleotide); some of the building blocks creating the long polymeric nucleic acid molecules.

For this purpose, two experiments were performed. The first experiment focused on examining the sensor resistance response to continual change of the gate voltage resulting in obtaining so-called transfer curves exhibiting peaks in resistance. The shift of these peaks indicates the doping by the molecules adsorbed on the graphene. The second experimental setup consisted of tracking the resistance response to the addition of various analyte solutions in real-time.

The gate voltage dependent response of the sensor was investigated in two distinguished FET configurations, top-gated and back-gated. These configurations differ in how the gate electrode is realized, either by a wire inserted into the electrolyte or by a solid-state substrate separated by a dielectric from the channel and source and drain electrodes.

Both of the performed experiments, the transfer curve measurements and real-time sensor response measurements, in their entirety, revealed that the cytosine-based substances impose an n-doping effect on the graphene channel. This way, it was possible to detect the presence of the analyte molecules and monitor the noticeable changes in the sensor response for different concentrations.

The effect that the gate-graphene distance in the top-gated configuration has on the sensor response was also examined. It was shown that while approaching the gate to the graphene surface, the response was unaffected only to a certain point from which the closer the gate was, the bigger drop in resistance was observed.

This work contributes to the understanding of the interactions of graphene with nucleic acid molecules, which is crucial for the use of graphene-based sensors as, for example, DNA hybridization detectors presented in the literature research part of this work. The use of such sensors has potential in the field of personalized medicine and is key to the diagnosis of genetic diseases. Further research follow-up to findings in this

work can also be directed at how the top gate shape, material and distance from the conductive graphene channel effects the sensor response.

Bibliography

[1] Wallace, P. R.: The Band Theory of Graphite. *Physical Review*, 1947: p. 622–634.

[2] Novoselov, K. S.; Geim, A. K.; Morozov, S. V.; et al.: Electric Field Effect in Atomically Thin Carbon Films. *Science*, vol. 306, 2004: p. 666–669, ISSN 0036-8075, doi:10.1126/science.1102896.

[3] Ponor: Carbon hybrid orbitals. 2020, wikimedia Commons, [Online]. URL `<https://en.wikipedia.org/wiki/File:Carbon_hybrid_orbitals_-_from_s%2Bpx,py,pz_to_sp%C2%B2%2Bpz.svg#/media/File:Carbon_hybrid_orbitals_-_from_s+px,py,pz_to_sp%C2%B2+pz.svg>`

[4] Ponor: Graphene - sigma and pi bonds. 2020, wikimedia Commons, [Online]. URL `<https://commons.wikimedia.org/wiki/File:Graphene_-_sigma_and_pi_bonds.svg#/media/File:Graphene_-_sigma_and_pi_bonds.svg>`

[5] Papageorgiou, D. G.; Kinloch, I. A.; Young, R. J.: Mechanical properties of graphene and graphene-based nanocomposites. *Progress in Materials Science*, vol. 90, 2017: p. 75–127, ISSN 0079-6425, doi:10.1016/j.pmatsci.2017.07.004.

[6] Savage, N.: Materials science: Super carbon. *Nature*, vol. 483, 2012, ISSN 0028-0836, doi:10.1038/483S30a.

[7] Lee, C.; Wei, X.; Kysar, J.; et al.: Measurement of the Elastic Properties and Intrinsic Strength of Monolayer Graphene. *Science*, vol. 321, 2008: p. 385–388, ISSN 0036-8075, doi:10.1126/science.1157996.

[8] Reddy, D.; Register, L. F.; Carpenter, G. D.; et al.: Graphene field-effect transistors. *Journal of Physics D: Applied Physics*, vol. 45, 2011: p. 313001, ISSN 1361-6463, doi:10.1088/0022-3727/44/31/313001.

[9] Biró, L. P.; Nemes-Incze, P.; Lambin, P.: Graphene: Nanoscale processing and recent applications. *Nanoscale*, vol. 4, 2012: p. 1824–1839, ISSN 2040-3372, doi:10.1039/c1nr11067e.

[10] Chen, J. H.; Jang, C.; Xiao, S.; et al.: Intrinsic and extrinsic performance limits of graphene devices on SiO_2. *Nature Nanotechnology*, vol. 3, 2008: p. 206–209, ISSN 1748-3387, doi:10.1038/nnano.2008.58.

[11] Baladin, A. A.; Hgosh, S.; Bao, W.; et al.: Superior Thermal Conductivity of Single-Layer Graphene. *Nano Letters*, vol. 8, 2008, doi:10.1021/nl0731872.

[12] Murali, R.; Yang, Y.; Brenner, K.; et al.: Breakdown Current Density of Graphene Nano Ribbons. *Applied Physics Letters*, vol. 94, 2009, doi:10.1063/1.3147183.

[13] Novoselov, K. S.; Geim, A. K.; Morozov, S. V.; et al.: Two-dimensional gas of massless Dirac fermions in graphene. *Nature*, vol. 438, 2005: p. 197–200, doi:10.1038/nature04233.

[14] Nair, R. R.; Blake, P.; Grigorenko, A. N.; et al.: Fine Structure Constant Defines Visual Transparency of Graphene. *Science*, vol. 320, 2008: p. 1308, doi:10.1126/science.1156965.

[15] Abergel, D. S. L.; Russell, A.; Fal'ko, V. I.: Visibility of graphene flakes on a dielectric substrate. *Applied Physics Letters*, vol. 91, 2007, doi:10.1063/1.2768625.

[16] Seekaew, Y.; Arayawut, O.; Timsorn, K.; et al.: Synthesis, Characterization, and Applications of Graphene and Derivatives. In *Carbon-Based Nanofillers and Their Rubber Nanocomposites*, ed. by S. Yaragalla; R. Mishra; S. Thomas; N. Kalarikkal; H. J. Maria, Elsevier, 2019, ISBN 978-0-12-813248-7, p. 259–283, doi:https://doi.org/10.1016/B978-0-12-813248-7.00009-2.

[17] Saeed, M.; Alshammari, Y.; Majeed, S. A.; et al.: Chemical Vapour Deposition of Graphene - Synthesis, Characterisation, and Applications: A Review. *Molecules*, vol. 25, 2020, doi:10.3390/molecules25173856.

[18] Chen, X.; Zhang, L.; Chen, S.: Large area CVD growth of graphene. *Synthetic Metals*, vol. 210, 2015: p. 95–108, ISSN 0379-6779, doi:10.1016/j.synthmet.2015.07.005.

[19] Terasawa, T.; Saiki, K.: Growth of graphene on Cu by plasma enhanced chemical vapor deposition. *Carbon*, vol. 50, 2012: p. 869–874, ISSN 0008–6223, doi:10.1016/j.carbon.2011.09.047.

[20] Yi, M.; Shen, Z.: A review on mechanical exfoliation for scalable production of graphene. *Journal of Materials Chemistry A*, vol. 3, 2015, doi:10.1039/C5TA00252D.

[21] Liangchuan, L.; Zhou, M.; Jin, L.; et al.: Research Progress of the Liquid-Phase Exfoliation and Stable Dispersion Mechanism and Method of Graphene. *Frontiers in Materials*, vol. 6, 2019, doi:10.3389/fmats.2019.00325.

[22] de Heer, W. A.; Berger, C.; Ruan, M.; et al.: Large area and structured epitaxial graphene produced by confinement controlled sublimation of silicon carbide. *Proceedings of the National Academy of Sciences*, vol. 108, 2011, ISSN 0027-8424, doi:10.1073/pnas.1105113108.

[23] Pinto, H.; Markevich, A.: Electronic and electrochemical doping of graphene by surface adsorbates. *Beilstein Journal of Nanotechnology*, vol. 5, 2014, doi:10.3762/bjnano.5.195.

[24] Lu, A. K. A.; Houssa, M.; Radu, I.; et al.: Towards an understanding of the electric field-induced electrostatic doping in Van der Waals heterostructures: a first-principles study. *ACS Applied Materials Interfaces*, vol. 9, 2017, doi:10.1021/acsami.6b14722.

[25] Liu, H.; Liu, Y.; Zhu, D. B.: Chemical doping of graphene. *Journal of Materials Chemistry*, vol. 21, 2011: p. 3335–3345, doi:10.1039/C0JM02922J.

[26] Lafkioti, M.; Krauss, B.; Lohmann, T.; et al.: Graphene on a Hydrophobic Substrate: Doping Reduction and Hysteresis Suppression under Ambient Conditions. *Nano Letters*, vol. 10, 2010: p. 1149–1153, doi:10.1021/nl903162a.

[27] Bartošík, M.; Mach, J.; Piastek, J.; et al.: Mechanism and Suppression of Physisorbed-Water-Caused Hysteresis in Graphene FET Sensors. *ACS Sensors*, vol. 5, 2020: p. 2940–2949, doi:10.1021/acssensors.0c01441.

[28] Soukup, G. A.: Nucleic Acids: General Properties. *Encyclopedia of Life Sciences*, 2001.

[29] Green, N. S.; Norton, M. L.: Interactions of DNA with graphene and sensing applications of graphene field-effect transistor devices: A review. *Analytica Chimica Acta*, vol. 853, 2015: p. 127–142, ISSN 0003-2670, doi:10.1016/j.aca.2014.10.023.

[30] Lee, J.; Choi, Y.; Kim, H.; et al.: Physisorption of DNA nucleobases on h-BN and graphene: VdW-corrected DFT calculations. *Journal of Physical Chemistry C*, vol. 117, 2013: p. 13435–13441, doi:10.1021/jp402403f.

[31] Gowtham, S.; Scheicher, R.; Ahuja, R.; et al.: Physisorption of nucleobases on graphene: Density-functional calculations. *Physical Review B - Condensed Matter and Materials Physics*, vol. 76, 2007, doi:10.1103/PhysRevB.76.033401.

[32] Boušek, J.; Kosina, P.; Mojrová, B.: *Elektronické součástky*. Vysoké učení technické v Brně, 2015.

[33] Béraud, A.; Sauvage, M.; Bazán, C. M.; et al.: Graphene field-effect transistors as bioanalytical sensors: design, operation and performance. *Analyst*, vol. 146, 2021: p. 403–428, doi:10.1039/D0AN01661F.

[34] Das, A.; Pisana, S.; Chakraborty, B.; et al.: Monitoring dopants by Rama scattering in an electrochemically top-gated graphene transistor. *Nature Nanotechnology*, vol. 3, 2008: p. 210–215, doi:10.1038/nnano.2008.67.

[35] Butt, H. J.; Karlheinz, G.; Kappl, M.: *Physics and Chemistry of Interfaces*. Wiley-VCH Verlag Co. KGaA, 2003.

[36] Saltzgaber, G.; Wojcik, P.; Sharf, T.; et al.: Scalable graphene field-effect sensors for specific protein detection. *Nanotechnology*, vol. 24, 2003, doi:10.1088/0957-4484/24/35/355502.

[37] Huard, B.; Stander, N.; Sulpizio, J. A.; et al.: Evidence of the role of contacts on the observed electron-hole asymmetry in graphene. *Physical Review B*, vol. 78, 2008, doi:10.1103/PhysRevB.78.121402.

[38] Dong, X.; Shi, Y.; Huang, W.; et al.: Electrical detection of DNA hybridization with single-base specificity using transistors based on CVD-grown graphene sheets. *Advanced Materials*, vol. 22, 2010: p. 1649–1653, doi:10.1002/adma.200903645.

[39] Danielson, E.; Sontakke, V.; Porkovich, A.; et al.: Graphene based field-effect transistor biosensors functionalized using gas-phase synthesized gold nanoparticles. *Sensors and Actuators, B: Chemical*, vol. 320, 2020, doi:10.1016/j.snb.2020.128432.

[40] Hwang, M. T.; Heiranian, M.; Kim, Y.; et al.: Ultrasensitive detection of nucleic acids using deformed graphene channel field effect biosensors. *Nature Communications*, vol. 11, 2020, doi:10.1038/s41467-020-15330-9.

[41] Xu, S.; Jiang, S.; Zhang, C.; et al.: Ultrasensitive label-free detection of DNA hybridization by sapphire-based graphene field-effect transistor biosensor. *Applied Surface Science*, vol. 427, 2018: p. 1114–1119, doi:10.1016/j.apsusc.2017.09.113.

[42] Xia, Y.; Sun, Y.; Li, H.; et al.: Plasma treated graphene FET sensor for the DNA hybridization detection. *Talanta*, vol. 223, 2021, doi:10.1016/j.talanta.2020.121766.

[43] Ping, J.; Vishnubhotla, R.; Vrudhula, A.; et al.: Scalable Production of High-Sensitivity, Label-Free DNA Biosensors Based on Back-Gated Graphene Field Effect Transistors. *ACS Nano*, vol. 10, 2016: p. 8700–8704, doi:10.1021/acsnano.6b04110.

[44] Malard, L.; Pimenta, M.; Dresselhaus, G.; et al.: Raman spectroscopy in graphene. *Physics Reoports*, vol. 473, 2009: p. 51–87, doi:10.1016/j.physrep.2009.02.003.

[45] Supalová L.: *Detection of biochemical substance using graphene sensor*. Brno, 2021, 52 p. Bachelor's Thesis. Brno University of Technology, Faculty of Mechanical Engineering, Institute of Physical Engineering.

List of symbols, quantities and abbreviations

Au ..... gold/golden

C ..... cytosine

CMP ..... cytidine monophosphate

Cu ..... copper

CVD ..... chemical vapour deposition

D ..... drain

dC ..... deoxycytidine

DFT ..... density functional theory

DI ..... deionized

DNA ..... deoxyribonucleic acid

DOS ..... density of states

EDL ..... electrical double layer

FET ..... field-effect transistor

FE(NO_3)$_3$ .... iron(III) nitrate

G ..... gate

GFET ..... graphene field-effect transistor

HCl ..... hydrochloric acid

HOMO ..... highest occupied molecular orbital

IPA ..... isopropyl alcohol

LUMO ..... lowest unoccupied molecular orbital

PMMA ..... poly(methyl methacrylate)

RNA ..... ribonucleic acid

S ..... source

SiO_2 ..... silicon dioxide

UV ..... ultra-violet

E_F ..... Fermi level

E_{redox} ..... electrochemical redox potential

I_{DS} ..... source-drain current

V_D ..... Dirac point voltage

V_{DS} ..... source-drain voltage

V_G ..... gate voltage

λ_D ..... Debye length